

The Coupled Manifold

A. NAVARRA

INGV, Bologna, Italy

J. TRIBBIA

NCAR, Boulder, Colorado

(Manuscript received 5 February 2004, in final form 25 June 2004)

ABSTRACT

A new method is presented to detect the portion of variability connected between two climatic fields. The method is a realization of the Procrustes problem, and it is a generalization of methods for analysis of variance such as the singular value decomposition (SVD) or canonical correlation analysis (CCA). The Procrustes formulation offers a general framework to link together variance analysis methods, and regression methods, including as special cases SVD and CCA.

Using this approach two fields can be divided into a subspace where variations of one field are connected to variations of the other field, the coupled manifold, and a subspace where variations are independent, the free manifold. The unified approach can be applied to prescribed SST experiments, in which case it recovers consistent results with other methods designed to identify the forced portion of variance, but it can now be extended also to the coupled case or to observations.

Some examples from prescribed SST simulation experiments and observations are discussed.

1. Introduction

The climate system is a complex web of interactions and feedbacks. Scientific understanding of its evolution can be advanced only by unraveling the interactions between the distinct parameters that we can observe and measure. It is not surprising, then, that the attention of the investigators has been focused on developing ways to identify interacting variables and quantify their interaction or coupling. The sea surface temperature (SST) and its interaction with atmospheric fields is one of the most prominent cases of such an intense relation, but it is not the only one. However, in the following we will be using the SST-related influence and coupling as the test bed for our analysis.

The effect of SST on climate variability has been demonstrated in the past 20 years using increasingly sophisticated models and realistic experimental numerical simulations. Experiments were performed initially using idealized SST anomalies (Rowntree 1972). Later, the pioneering experiments of Lau (1985), with monthly varying observed SST, paved the way for such experimental settings to become commonplace in numerical simulation groups (Lau and Nath 1990, 1994;

Gates 1992; Harzallah and Sadourny 1995; Graham et al. 1994; Kumar et al. 1996; Rowell 1998). Observational studies have shown the near-global influence of the El Niño–Southern Oscillation (ENSO; Ropelewski and Halpert 1987, 1989; Kiladis and Diaz 1989), and the SST is now accepted as an important factor in influencing the global climate variability, generating reproducible—that is, predictable—signals (Stern and Miyakoda 1995; Barnett 1995; Sperber and Palmer 1996).

The general vision of the processes through which the SST affects climate variability is expressed by dividing the atmospheric variability in two parts (Rowell 1998): a portion that is directly connected to the SST and a second portion composed by internal modes of variations of the atmosphere. The second portion is sometimes called “free modes,” because they should be present also in the absence of SST variability. The variance of the two sectors can be estimated by statistical techniques, but those methods yield bulk estimates in percentage of variance “explained” by the SST forcing rather than the anomaly pattern forced by the SST itself. It would be desirable to have a way to study separately anomalies forced by the SST or the free modes. The situation is made even more complicated by the fact that though the SST is a major forcing agent, there are others mechanisms active at the same time in the climate system that can create their own variability.

Several approaches have been discussed mainly in

Corresponding author address: A. Navarra, INGV, Via Creti 12, 40129 Bologna, Italy.
E-mail: navarra@bo.ingv.it

the context of ensemble experiments with prescribed SST (Rowell 1998; Shukla et al. 2000). The free variability is thought to be more stochastic in nature than the forced components, being mainly regulated by the internal nonlinear interaction of the atmosphere. Ensemble experiments, in which several simulations are realized with the same forcing (often just the SST), but otherwise randomly perturbed initial conditions, are designed to isolate the SST-related variability. The underlying assumption is that the forced signal will be similar in all experiments, whereas the free component will be stochastic and therefore removable by statistical methods. Relatively less attention has been given to the problem of separating the variability in the context of coupled systems. The coupled system poses some new challenges, since the ensemble approach has to be redefined to be able to extract the part of variability linked to SST.

A wide set of analysis methods has been devoted to assist in such investigations. Bretherton et al. (1992) listed a number of approaches based on the analysis of variance to identify patterns of covariation. The methods that can be applied to the covariation of two fields have been extensively applied to investigate the effects of SST on various atmospheric fields. The basic idea is to extend the concept of empirical orthogonal functions (EOFs) to cross-covarying fields using singular value decomposition (SVD) to maximize explained covariance or canonical correlation analysis (CCA) to maximize correlations. However, some reservations have been raised about the effectiveness of these methods in really identifying relations of influence between fields, especially for the SVD method when it is used to identify the operator connecting two fields (Newman and Sardeshmukh 1995) and Cherry (1996).

In this paper we discuss this issue by concentrating on the relations between atmospheric anomalies and SST anomalies, focusing on anomalies that are highly correlated with the SST variability. We will call the set of states that are linked to SST in the context of ensembles of prescribed SST experiments the “forced manifold.”

This concept will help us to make the transition to coupled models or observed data where ensembles cannot be defined and the method to capture the covariance of fields—for instance, between the SST and other atmospheric fields—become elusive. We are able to show that we can extend the concepts and the methods used for the forced manifold, identifying what might be called the “coupled manifold.” We initially discuss the various ways in which such relations have been analyzed in the previous studies and then we define a simple procedure to identify the coupled manifold in ensemble simulations and in coupled simulations.¹

The paper is organized as follows. Section 2 discusses

the various techniques that identify the relations between SST and atmospheric fields, section 3 introduces the coupled manifold, and section 4 discusses the coupled manifold in the particular case of ensemble simulations. Section 5 contains some examples of the coupled manifold concept applied to some simulation experiments; and some conclusive remarks are contained in section 6.

2. Detecting cross-influences of fields

a. The Procrustes method

Atmospheric and oceanic fields influence each other, and in very general terms, the relation can be conceptualized as a functional relation,

$$\mathbf{Z} = f(\mathbf{S}), \quad (1)$$

where the atmospheric variable has been denoted by \mathbf{Z} and the oceanic variable by \mathbf{S} . The exact form of the relation is unknown, but it is probably time dependent and thus includes effects of time lags and so on. In practice, the investigations have often assumed a simpler form for (1). They have concentrated on the instantaneous relation at a certain fixed time and they have assumed a linear form for the functional dependence. Powerful methods have been devised for identifying relations of the form (1) assuming that $f(\mathbf{S})$ is a linear function, starting from linear correlation methods, teleconnection analysis, and finally culminating with methods to analyze systematically the linear relations between the two datasets, such as the SVD or CCA. SVD has been used before in meteorological applications (Brier and Meltesen 1976), but it was proposed by Bretherton et al. (1992) as a method to analyze cross correlation between different fields. Further analysis showed that the SVD is determined up to a rotation (Horn and Johnson 1991; Newman and Sardeshmukh 1995; Hu 1997; Cheng and Dunkerton 1995; Cherry 1996, 1997) and therefore the physical interpretation of the modes themselves must proceed with caution. Furthermore, some doubts were cast on its ability to truly identify the couplings.

Assuming linearity, the relation between the fields \mathbf{Z} and \mathbf{S} can be written as

$$\mathbf{Z}(t) = \mathbf{A}\mathbf{S}(t), \quad (2)$$

where the operator \mathbf{A} is the coupling linear operator and it is assumed here to be stationary. If we have data at discrete times from observations or simulations, the equation can be written in terms of data matrices \mathbf{Z} and \mathbf{S} as

$$\mathbf{Z} = \mathbf{A}\mathbf{S}, \quad (3)$$

where

$$\begin{aligned} \mathbf{Z} &= [\mathbf{z}(1), \mathbf{z}(2), \dots, \mathbf{z}(n)], \\ \mathbf{S} &= [\mathbf{s}(1), \mathbf{s}(2), \dots, \mathbf{s}(n)] \end{aligned} \quad (4)$$

¹ MATLAB codes for the calculation of the manifolds are available upon request from the authors.

are data matrices describing the atmospheric and oceanic fields at fixed times, and \mathbf{A} is the matrix representation of the linear relations. The spatial points need not to be the same in the \mathbf{Z} and \mathbf{S} data and so the two matrices will be in general rectangular matrices, with n columns and, respectively, p rows for \mathbf{Z} and q rows for \mathbf{S} .

It is possible to set a simple minimization problem for \mathbf{A} , as

$$\min \|\mathbf{Z} - \mathbf{AS}\|_F^2, \quad (5)$$

where the norm is the Frobenius norm, defined by

$$\|\mathbf{Z}\|_F^2 = \text{trace}(\mathbf{ZZ}'), \quad (6)$$

and the apex $()'$ denotes the transpose. The minimization problem (5), a kind of least squares problem, is known in the mathematical literature as the “Procrustes problem” (Richman and Vermette 1993). A solution can be written as

$$\mathbf{A} = \mathbf{ZS}'(\mathbf{SS}')^{-1}. \quad (7)$$

If \mathbf{SS}' is of full rank, the solution is exact and the inverse exists, otherwise a minimization solution can still be found by using a pseudoinverse. The pseudoinverse is not unique, but in the following we use the Penrose definition (Golub and van Loan 1989). The Penrose pseudoinverse is defined in terms of the eigenmodes u_i of the matrix \mathbf{SS}' as

$$(\mathbf{SS}')^{-1} = \sum_{i=1}^k u_i \lambda_i^{-1} u_i', \quad (8)$$

where the summation extends over all nonzero eigenvalues/eigenvectors of the matrix. In this way modes that do not contribute to the variance of \mathbf{S} are excluded from the inverse.

The operator \mathbf{A} is the mathematical representation of the functional relation between fields; it can be understood as the operation that transforms the \mathbf{S} fields into \mathbf{Z} . The strength of the relation depends on the value of the minimum. In the case of an exact solution—that is, the minimum is zero—then there is a linear relation \mathbf{A} that links the entire field \mathbf{Z} to \mathbf{S} . If the minimum is not zero, then it is only a portion of the field \mathbf{Z} variability that can be associated with the variability of \mathbf{S} .

We have no reason, however, to pose the problem as (3) rather than as the sister problem:

$$\mathbf{S} = \mathbf{BZ}, \quad (9)$$

in which we are trying to express \mathbf{S} in terms of \mathbf{Z} and for which we obtain an analogous minimization solution

$$\mathbf{B} = \mathbf{SZ}'(\mathbf{ZZ}')^{-1}. \quad (10)$$

We now have two operators, \mathbf{A} and \mathbf{B} , that express the relation between \mathbf{S} and \mathbf{Z} , but they are not completely equivalent. The operator \mathbf{A} can be interpreted as expressing the influence of \mathbf{S} in terms of \mathbf{Z} , whereas

the operator \mathbf{B} represents the influence of \mathbf{Z} on \mathbf{S} . The relation between \mathbf{A} and \mathbf{B} is rather tenuous, though they both involve the cross-correlation matrix \mathbf{ZS}' and its transpose \mathbf{SZ}' . In general there is no reason to expect them to have any special structure.

Further insight can be gained by realizing that (3) or (9) represents a multivariate regression problem for the atmospheric field \mathbf{Z} on the oceanic SST field \mathbf{S} . Following this interpretation, it is then possible to show that the solution (7) or (10) is the maximum likelihood solution of the regression problem. This is the most general formulation of the coupling problem, subject only to the constraint of linearity in the coupling, and it will give an indication of the strength of the relation between one field and the other. The method based on operators \mathbf{A} and \mathbf{B} obtained via the Procrustes method will be denoted in the following as the PRO method.

b. A practical, faster method

A significant simplification of the calculation can be readily achieved by transforming the data by calculating the respective EOFs beforehand and then using the EOF coefficients in the following analysis. In this case the data matrices become, where the tilde indicate the EOF coefficients,

$$\begin{aligned} \tilde{\mathbf{Z}} &= [\tilde{\mathbf{z}}(1), \tilde{\mathbf{z}}(2), \dots, \tilde{\mathbf{z}}(N)], \\ \tilde{\mathbf{S}} &= [\tilde{\mathbf{s}}(1), \tilde{\mathbf{s}}(2), \dots, \tilde{\mathbf{s}}(N)]. \end{aligned} \quad (11)$$

The PRO method can then be set up for the EOF coefficients:

$$\min \|\tilde{\mathbf{Z}} - \tilde{\mathbf{A}}\tilde{\mathbf{S}}\|_F^2. \quad (12)$$

The solution can then be obtained in terms of the tilde quantities:

$$\tilde{\mathbf{A}} = \tilde{\mathbf{Z}}\tilde{\mathbf{S}}'(\tilde{\mathbf{S}}\tilde{\mathbf{S}}')^{-1}. \quad (13)$$

The reduction of the mathematical dimension of the problem is quite significant. In the case of a geophysical field, the data matrices are usually very rectangular, because the length of the columns that describe the spatial extent of the field is usually much larger than the length of the rows that describe the number of time levels analyzed. The minimization problem is then quite tractable.

The use of EOFs also offers the possibility of an interpretation of the operators \mathbf{A} and \mathbf{B} . The operator \mathbf{A} is the matrix that expresses the contribution to a single mode of \mathbf{Z} , for instance, the first mode by all the modes of \mathbf{S} . By analyzing the columns of \mathbf{A} we can analyze the regression factor by which each mode of \mathbf{S} contributes to the that particular mode. Large values indicate a strong impact of that \mathbf{S} mode on the variability of the first \mathbf{Z} mode. The analysis can be repeated for each column, thereby reconstructing the map of the \mathbf{S} modes that have strong influences on \mathbf{Z} .

A similar argument can be done for the \mathbf{B} operator,

in which the role of \mathbf{S} and \mathbf{Z} are reversed. In this case the column will indicate which of the \mathbf{Z} modes contributed more strongly to the first \mathbf{S} mode. Together, the two operators contain a fairly detailed map of the influence patterns between the fields. The influence pattern is demonstrated in the following scheme, where the coefficients of the operator \mathbf{A} , each of them being a regression factor, are expressing the influence of the first \mathbf{S} mode on the first \mathbf{Z} mode ($\mathbf{S}_1 \rightarrow \mathbf{Z}_1$) or of the second mode on the first mode ($\mathbf{S}_2 \rightarrow \mathbf{Z}_1$) and so on:

$$= \begin{bmatrix} \mathbf{S}_1 \rightarrow \mathbf{Z}_1 & \mathbf{S}_2 \rightarrow \mathbf{Z}_1 & \dots & \mathbf{S}_n \rightarrow \mathbf{Z}_1 \\ \mathbf{S}_1 \rightarrow \mathbf{Z}_2 & \dots & \dots & \dots \\ \dots & \dots & \dots & \mathbf{S}_n \rightarrow \mathbf{Z}_n \end{bmatrix} \quad (14)$$

The \mathbf{B} operator can be interpreted in a similar way, with the role of \mathbf{Z} and \mathbf{S} reversed. Now the (1,1) element of \mathbf{B} expresses the influence of the first \mathbf{Z} mode on the first \mathbf{S} mode ($\mathbf{Z}_1 \rightarrow \mathbf{S}_1$) or of the second mode on the first mode ($\mathbf{Z}_2 \rightarrow \mathbf{S}_1$) and so on:

$$= \begin{bmatrix} \mathbf{Z}_1 \rightarrow \mathbf{S}_1 & \mathbf{Z}_2 \rightarrow \mathbf{S}_1 & \dots & \mathbf{Z}_n \rightarrow \mathbf{S}_1 \\ \mathbf{Z}_1 \rightarrow \mathbf{S}_2 & \dots & \dots & \dots \\ \dots & \dots & \dots & \mathbf{Z}_n \rightarrow \mathbf{S}_n \end{bmatrix} \quad (15)$$

In principle, the usage of the EOF allows one to filter the data prior to the application of the PRO method by retaining only some of the EOF and achieving another significant saving. This is not required by the method itself but is a feature that adds further flexibility to the method and can be helpful in avoiding overfitting. The issue of neglecting certain EOFs is always a very delicate subject and should be carried out with a careful consideration of the specific problem. Some general criteria can be formulated (see, e.g., North et al. 1982), but especially in strongly nonlinear problems small variance does not always imply small importance.

c. A different scaling

It is interesting to note what happens when the data are scaled by the covariance matrices. If we take the data in the EOF representation and we scale them by the square root of their covariance matrices,

$$\begin{aligned} \hat{\mathbf{Z}} &= (\tilde{\mathbf{Z}}\tilde{\mathbf{Z}}')^{-1/2}\tilde{\mathbf{Z}}, \\ \hat{\mathbf{S}} &= (\tilde{\mathbf{S}}\tilde{\mathbf{S}}')^{-1/2}\tilde{\mathbf{S}}, \end{aligned} \quad (16)$$

then

$$\begin{aligned} \hat{\mathbf{S}}\hat{\mathbf{S}}' &= \mathbf{1}, \\ \hat{\mathbf{Z}}\hat{\mathbf{Z}}' &= \mathbf{1}. \end{aligned} \quad (17)$$

When this scaling is used the cross covariance matrix becomes the cross-correlation matrix. The minimization problem can then be written as

$$\begin{aligned} \hat{\mathbf{Z}} &= \hat{\mathbf{A}}\hat{\mathbf{S}}, \\ \hat{\mathbf{A}} &= \hat{\mathbf{Z}}\hat{\mathbf{S}}'(\hat{\mathbf{S}}\hat{\mathbf{S}}')^{-1} = \hat{\mathbf{Z}}\hat{\mathbf{S}}'. \end{aligned} \quad (18)$$

Interestingly the sister problem can be solved as

$$\begin{aligned} \hat{\mathbf{S}} &= \hat{\mathbf{B}}\hat{\mathbf{Z}}, \\ \hat{\mathbf{B}} &= \hat{\mathbf{S}}\hat{\mathbf{Z}}'(\hat{\mathbf{Z}}\hat{\mathbf{Z}}')^{-1} = \hat{\mathbf{S}}\hat{\mathbf{Z}}', \end{aligned} \quad (19)$$

and therefore

$$\hat{\mathbf{B}} = \hat{\mathbf{A}}'. \quad (20)$$

In this scaling the interaction matrices \mathbf{A} and \mathbf{B} are the transpose one of the other. This means that only one matrix is sufficient to describe the interaction among the various modes. The upper half of the matrix describes in this case the influence of \mathbf{Z} on \mathbf{S} and the lower half the influence of \mathbf{S} on \mathbf{Z} . This scaling is used in the canonical correlation analysis approach, and this relation prompts us to examine what are the connections between the PRO methods and the other methods used to analyze variance.

3. The relation between the PRO method and the other methods

It is interesting to analyze what happens if further restrictions are put on the coupling matrix \mathbf{A} . If we require that \mathbf{A} be an orthogonal matrix \mathbf{Q} — $\mathbf{Q}\mathbf{Q}' = \mathbf{Q}'\mathbf{Q} = \mathbf{1}$ —then we obtain the orthogonal Procrustes problem,

$$\min \|\mathbf{Z} - \mathbf{Q}\mathbf{S}\|_F^2. \quad (21)$$

The solution is given by (Golub and van Loan 1989)

$$\mathbf{Q} = \mathbf{U}\mathbf{V}', \quad (22)$$

where the \mathbf{U} and \mathbf{V} are obtained by the singular value decomposition of the cross-correlation matrix

$$\mathbf{Q} = \mathbf{Z}\mathbf{S}'. \quad (23)$$

This is the definition of the SVD method as proposed by Bretherton et al. (1992), and we can now see that it is essentially a Procrustes problem, with the requirement that the coefficient matrix be orthogonal. This result is consistent with Cherry (1996), who found that SVD is essentially trying to rotate one dataset into the other. Searching coupled modes with SVD is therefore equivalent to assuming a priori that the coupling relation between the fields is special.

Similarly, it is possible to realize that the canonical correlation analysis is the related problem

$$\min \|\tilde{\mathbf{Z}} - \tilde{\mathbf{Q}}\tilde{\mathbf{S}}\|_F^2. \quad (24)$$

where the data matrices have been previously scaled as

$$\begin{aligned} \tilde{\mathbf{Z}} &= (\mathbf{Z}\mathbf{Z}')^{-1/2}\mathbf{Z}, \\ \tilde{\mathbf{S}} &= (\mathbf{S}\mathbf{S}')^{-1/2}\mathbf{S}, \end{aligned} \quad (25)$$

and a similar requirement of orthogonality for \mathbf{Q} is imposed.

From this point of view is not surprising that identification of coupled modes via SVD or CCA is sometimes arduous, since the orthogonality constraint for the influence operators does not seem to have any physical justification.

4. An idealized example

It is possible to have a measure of the capability of the Procrustes method by performing a simple experiment with synthetic data. We will apply the procedure to a set of two-dimensional functions, represented by 10×10 random data matrices at times $1, 2, \dots, N$. A dataset is constructed unrolling each two-dimensional field into a vector of dimension 100 and putting the data in a bigger matrix \mathbf{Z} ,

$$\mathbf{Z} = [\mathbf{z}(1), \mathbf{z}(2), \dots, \mathbf{z}(N)], \quad (26)$$

then a Laplacian operator is applied to each two-dimensional field and the result is unrolled again to obtain another big matrix \mathbf{S} , indicated schematically as

$$\mathbf{S} = \nabla^2[\mathbf{z}(1), \mathbf{z}(2), \dots, \mathbf{z}(N)]. \quad (27)$$

We can use the Procrustes problem to attempt to recover the form of the Laplacian. This idealized experiment is reproducing a similar set up used by Newman and Sardeshmukh (1995) to test the SVD method. The results are shown in Fig. 1 where we have plotted the numerical representation of the Laplacian for the larger number of time levels for the data (100). The bottom panel shows the target Laplacian computed from the finite-difference form of the operator; the middle panel shows the reconstruction of the operator \mathbf{A} using the Procrustes' method with 10 samples, that is, 10 time levels (columns) in the data matrices; and the top panel shows the reconstruction of the \mathbf{B} operator, in this case the \mathbf{B} operator is obviously just the inverse Laplacian ∇^{-2} . Figure 2 shows the same patterns for the case of 100 samples. The reconstruction in this case is essentially perfect. Even in the case where only 10 samples were available it is possible to see the main structure of the Laplacian emerging in the \mathbf{A} operator, whereas the \mathbf{B} operator is difficult for the PRO method with this sample number. In this case the entire dataset in the matrix \mathbf{Z} is linked to the matrix \mathbf{S} , and the \mathbf{B} operator coincides with the inverse, or more precisely, the pseudoinverse. The structure in Fig. 2a corresponds to the inverse of the Laplacian in the numerical representation chosen.

The SVD approach is much less successful in identifying the operators. Figure 3 shows the result of applying the SVD approach to the test case. It is clear that the SVD has much more difficulty in identifying the operator connecting the two datasets. This result is a confirmation of a similar calculation performed by Newman and Sardeshmukh (1995). They tried (unsuccessful)

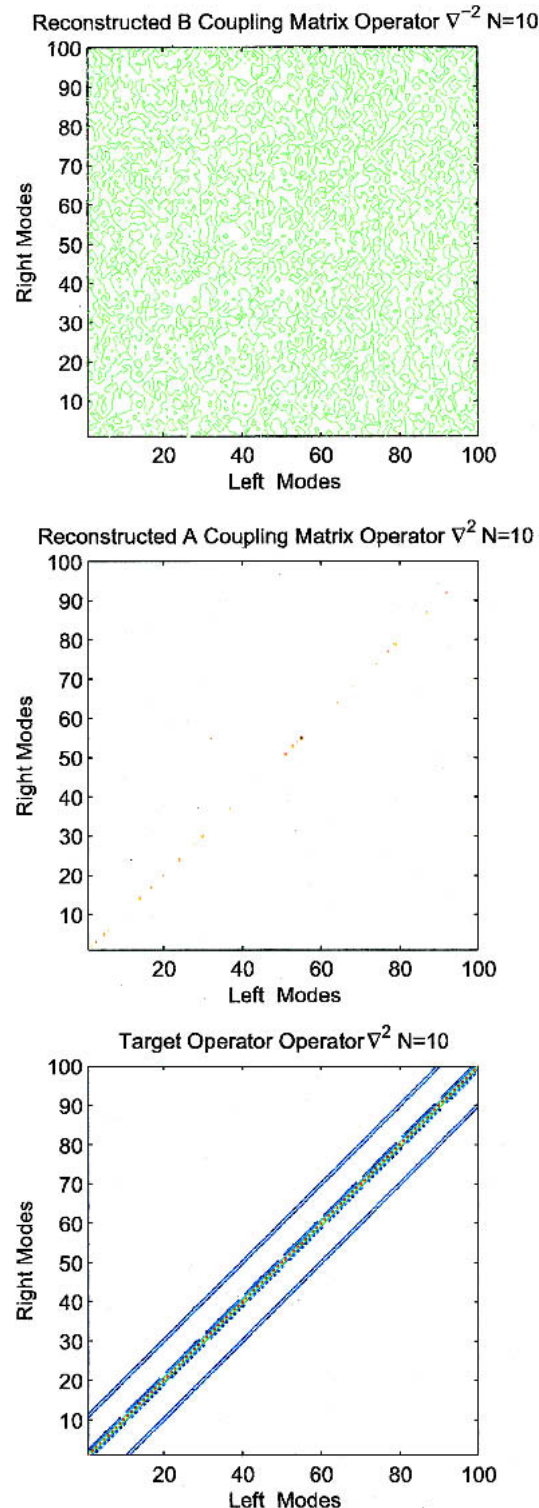


FIG. 1. Reconstruction of the numerical operator with the Procrustes problem, with a sample of dimension 10. (bottom) The matrix representation of the target Laplacian operator; (middle) the estimated operator for the \mathbf{Z} - \mathbf{S} problem; (top) the estimated operator for the \mathbf{S} - \mathbf{Z} problem. The panels show the matricial representation of the Laplacian used in the tests (4 along the main diagonal and -1 for the off-diagonals). The contour interval in the top panel is 0.1, and it is 0.5 for the middle and bottom panels.

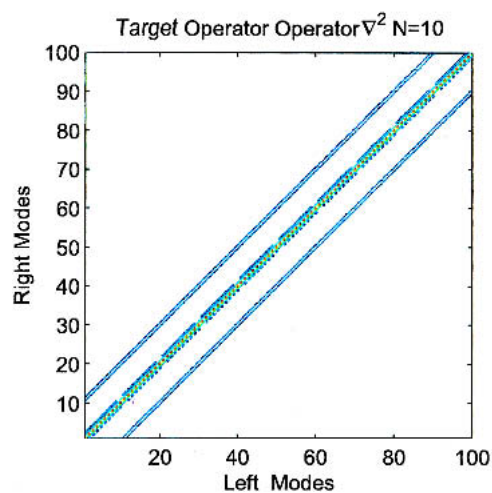
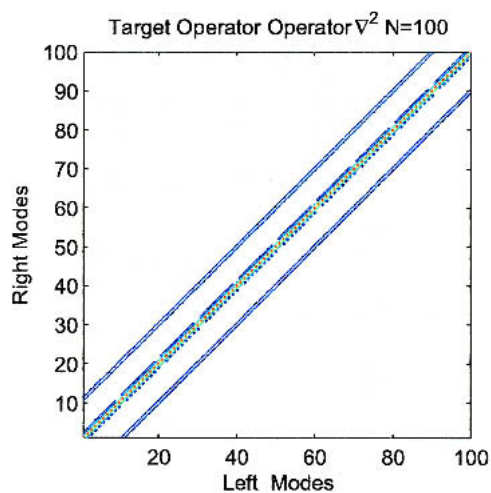
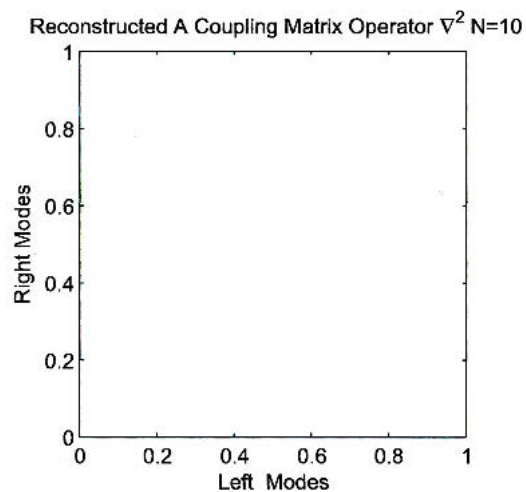
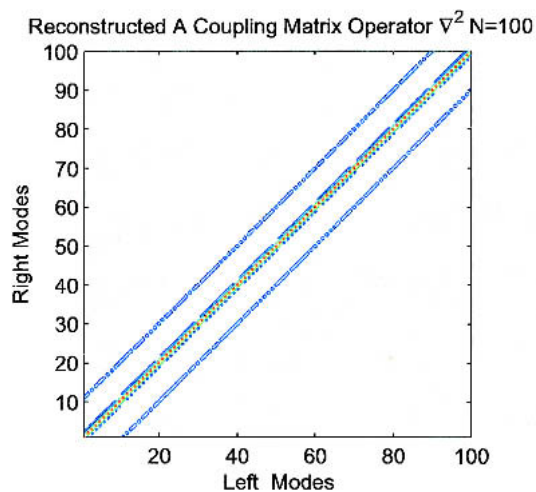
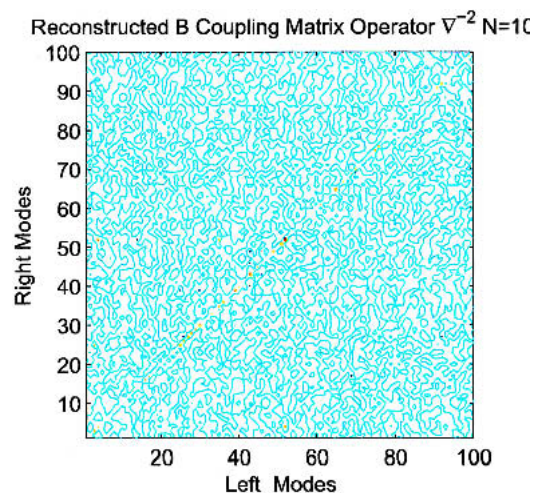
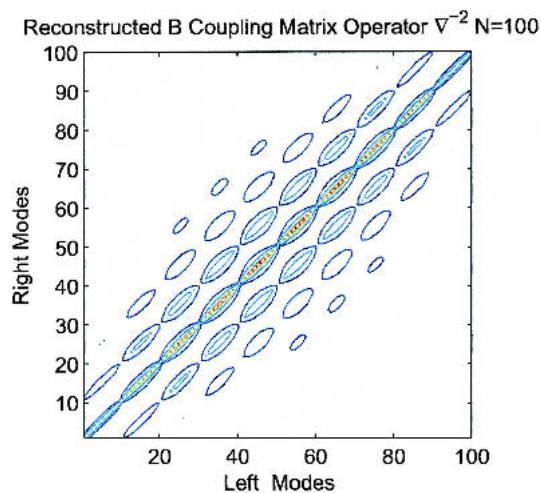


FIG. 2. As in Fig. 1, but for the case of a sampling dimension of 100.

FIG. 3. As in Fig. 1, but for the case of the orthogonal Procrustes problem, also known as the SVD analysis; sampling dimension is 10.

cessfully) to recover a Laplacian applying SVD to pairs of vorticity and streamfunction fields; our example shows how the PRO method can effectively reconstruct the form of the coupling operator from the datasets. In

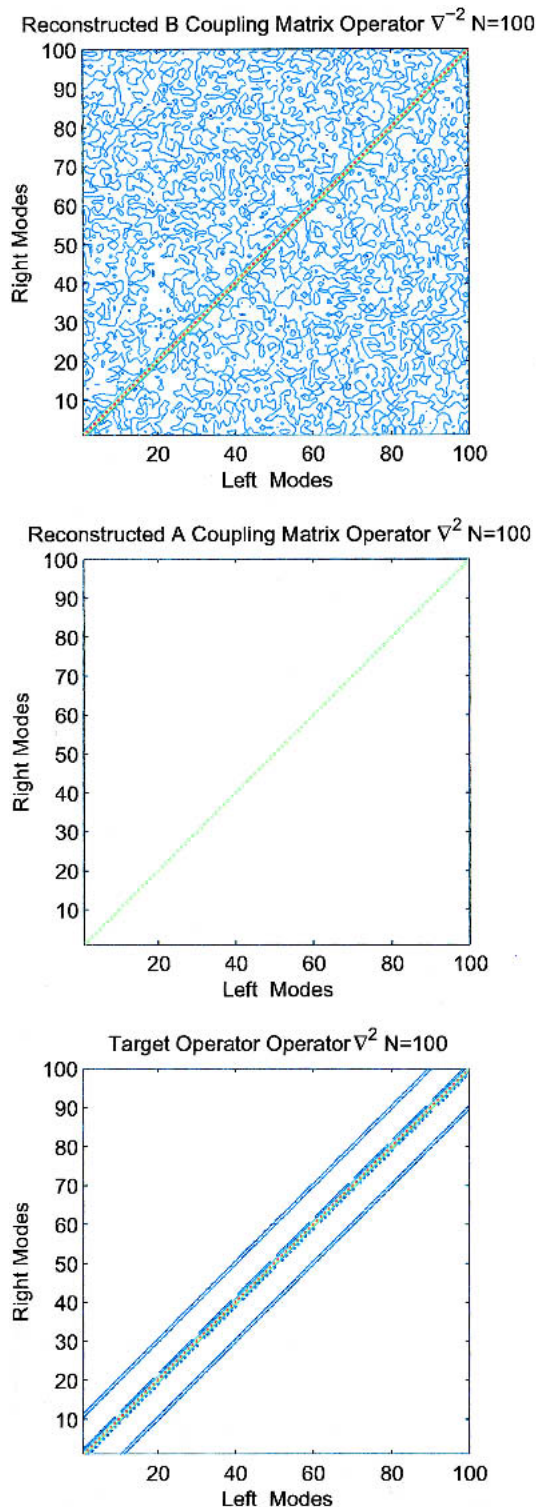


FIG. 4. As in Fig. 3, but for a sampling dimension of 100.

TABLE 1. The fit (norm of the difference between the estimated and target operators) for the test case (Laplacian) of Figs. 1 and 2 for different numbers of samples.

	$N = 10$	$N = 50$	$N = 80$	$N = 100$	$N = 200$
PRO	42	31	19	10^{-11}	10^{-13}
SVD	43	39	37	36	36

the case of high number of data samples [100 (see Fig. 4) and 200] the reconstruction can be done within numerical machine accuracy.

Table 1 shows in detail the development of the fit as the number of samples increase. The SVD cannot recover fully the operator, whereas the PRO method readily reconstructs the Laplacian operator. The PRO method works very well also in the case in which the operator used to create \mathbf{S} is just a random operator (Table 2), also in this case the fit index decreases very rapidly. It is possible to see that this case is harder for the SVD since the random operator is not symmetric and therefore the orthogonality requirement of the SVD is more inaccurate.

5. The case of prescribed SST ensemble experiments: The forced manifold

The residual predictability that can be hoped for at seasonal time scales has to come mainly from the effect of SST forcing and the other factors that can also play a role, like soil moisture, snow and ice cover, vegetation distribution and, possibly, the phase of the quasi-biennial oscillation (QBO). However, even the quest for SST-forced modes has proved to be elusive. Various techniques have been employed, ranging from correlation and teleconnection maps to variance analysis employing EOF and finally to cross-covariance analysis using CCA and SVD. We now tackle this problem with the PRO method. We will use datasets from prescribed SST simulations performed with our atmospheric GCM, ECHAM4 (Roeckner and Arpe 1995; Roeckner et al. 1996), at T30 resolution. The experiments are taken from an ensemble of prescribed SST experiments described in Moron et al. (1998) and Cherchi and Navarra (2003), using the SST compiled at the Hadley Centre (Rayner et al. 1996). We use the geopotential height at 200 mb as the \mathbf{Z} field and the SST as the \mathbf{S} field. The datasets are composed of three members for the period 1961–94. The PRO method is applied to the winter season averages for the period January–

TABLE 2. The fit (norm of the difference between the estimated and target operators) for the test case (random operator) of Figs. 1 and 2 for different numbers of samples.

	$N = 10$	$N = 50$	$N = 80$	$N = 100$	$N = 200$
PRO	53	41	23	10^{-8}	10^{-13}
SVD	54	55	54	54	54

February–March (JFM) according to the problems described in the previous sections. Each column of the \mathbf{Z} matrix will contain the unrolled geopotential for a winter season in a single vector, 34 columns for each member for the period 1961–94, in total 108 columns. The columns of the matrix \mathbf{S} contain the corresponding SST for the same winter unrolled in the same way, $\mathbf{Z} = [\mathbf{z}(1961); \text{First Member: } \mathbf{z}(1994), \mathbf{z}(1961); \text{Second Member: } \mathbf{z}(1994), \mathbf{z}(1961); \text{Third Member: } \mathbf{z}(1994)]$, whereas the SST is repeated for each member as $\mathbf{S} = [\mathbf{s}(1961); \mathbf{s}(1994), \mathbf{s}(1961); \mathbf{s}(1994), \mathbf{s}(1961); \mathbf{s}(1994)]$. We have used the fast (EOF) method and we have chosen to keep enough modes for SST and \mathbf{Z} corresponding to retaining 90% of the SST variance and 90% of the \mathbf{Z} variance.

The results are shown in Fig. 5. The top panels show the operators \mathbf{A} (right) and \mathbf{B} (left). It is possible to see some pattern in the coefficients involving a few modes. The absolute value of the coefficients tends to be larger for the higher modes to compensate for the typical drop

in absolute value that the coefficient of the higher modes shows. Large values of the coefficients are obtained for the lower modes in the case of the operator \mathbf{A} , which reconstruct the geopotential \mathbf{Z} from the SST, whereas the operator \mathbf{B} , which tries to realize the opposite operation to get the SST from the geopotential, has less structure. The geopotential reconstructed with the \mathbf{A} operator explains in general 29% of the total geopotential time variance, whereas the SST reconstructed via the operator \mathbf{B} explains 53% of the total SST variance.

If the CCA scaling is used (bottom panel), the differences between the coefficients become less pronounced and more uniform, reflecting the fact that the scaling puts the same modes on the same level by equalizing the contribution to the total variance. Only one panel is shown since in this case the \mathbf{B} operator is simply the transpose of \mathbf{A} .

Using the operator \mathbf{A} we can then separate the field \mathbf{Z} in two parts as

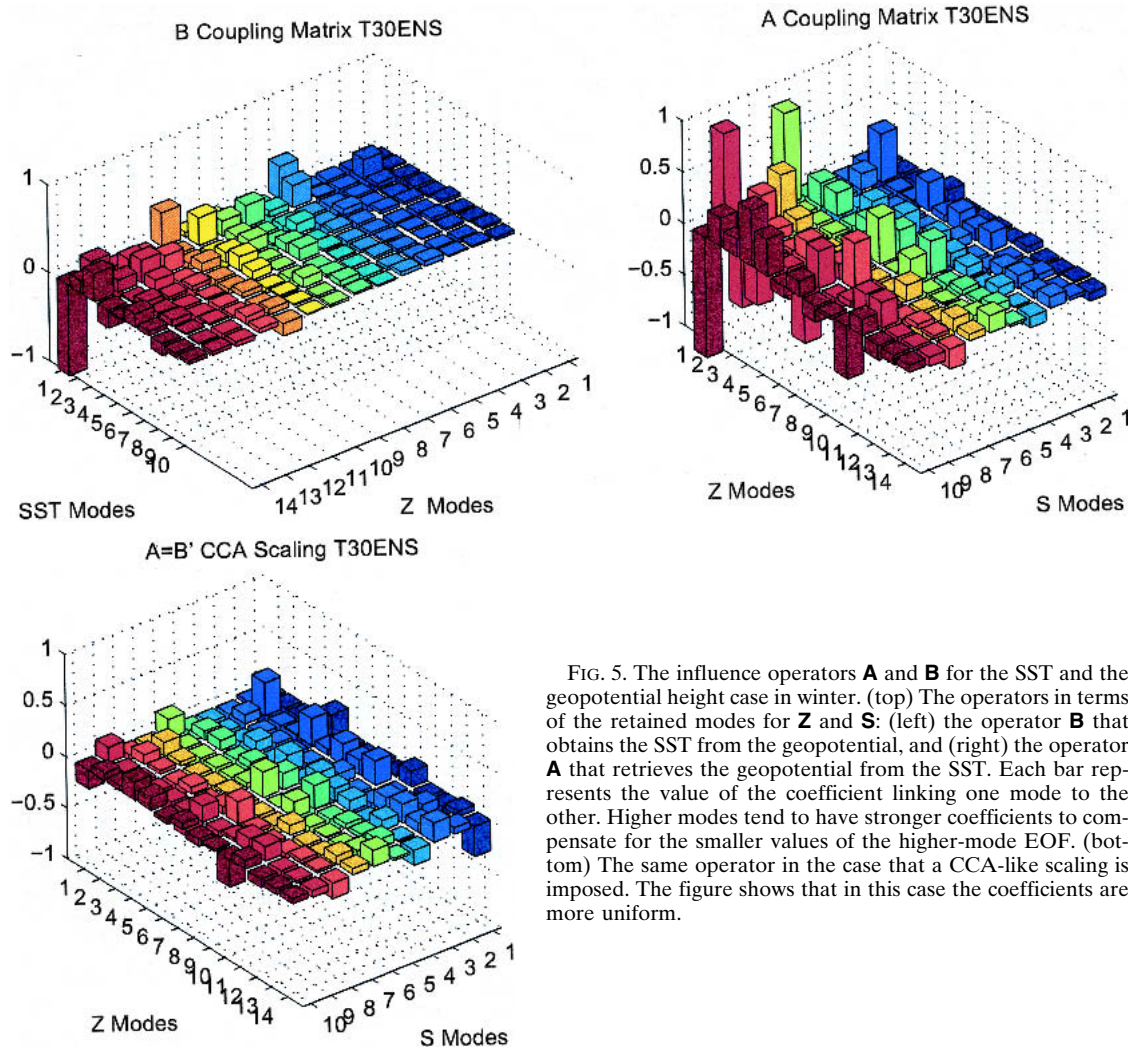


FIG. 5. The influence operators \mathbf{A} and \mathbf{B} for the SST and the geopotential height case in winter. (top) The operators in terms of the retained modes for \mathbf{Z} and \mathbf{S} : (left) the operator \mathbf{B} that obtains the SST from the geopotential, and (right) the operator \mathbf{A} that retrieves the geopotential from the SST. Each bar represents the value of the coefficient linking one mode to the other. Higher modes tend to have stronger coefficients to compensate for the smaller values of the higher-mode EOF. (bottom) The same operator in the case that a CCA-like scaling is imposed. The figure shows that in this case the coefficients are more uniform.

$$\begin{aligned} \mathbf{Z}_{\text{For}} &= \mathbf{AS}, \\ \mathbf{Z}_{\text{Free}} &= \mathbf{Z} - \mathbf{AS}. \end{aligned} \quad (28)$$

The \mathbf{Z}_{For} part is the portion of the field variability that is connected to the \mathbf{S} variability, whereas the \mathbf{Z}_{Free} is the part that is independent from \mathbf{S} . We will call the first part “forced manifold” and the second “free manifold.” The two parts are uncorrelated with each other as can be seen from

$$\mathbf{Z}_{\text{For}}' \mathbf{Z}_{\text{Free}}' = \mathbf{ZS}'(\mathbf{SS}')^{-1} \mathbf{S} [\mathbf{Z} - \mathbf{ZS}'(\mathbf{SS}')^{-1} \mathbf{S}]' = 0, \quad (29)$$

and the free manifold is uncorrelated with the SST

$$\mathbf{Z}_{\text{Free}}' \mathbf{S}' = (\mathbf{Z} - \mathbf{AS})' \mathbf{S}' = \mathbf{ZS}' - \mathbf{A}(\mathbf{SS}')', \quad (30)$$

but using the definition of \mathbf{A} in Eq. (13) we get

$$\mathbf{ZS}' - \mathbf{A}(\mathbf{SS}') = \mathbf{ZS}' - \mathbf{ZS}'(\mathbf{SS}')^{-1}(\mathbf{SS}') = 0, \quad (31)$$

showing that the free manifold has no correlation left with the SST.

The \mathbf{Z}_{For} part can be considered as forced by the SST and therefore we can see now how the name forced manifold is justified. It is composed of the variability that can be regressed to the SST in a linear sense. The residual \mathbf{Z}_{Free} is the free manifold of the modes that are independent from SST. The separation of the two fields is quite efficient, and a plot of the standard deviations for forced and free manifold will show complementary variance. Normalized anomalies have unity standard deviations in each point, and in this case the variance would split between the free and forced manifold in a clean way. The variance of the forced manifold would follow closely the pattern of the potential predictability computed using, for instance, the Rowell (1998) method, but in this case we will get a better separation of the field that we might get with the ensemble mean that does not completely remove residuals of correlation with the SST in the deviations from the ensemble mean part (Venzke et al. 1999).

Using the forced and free manifold concept we can separate the two fields as

$$\begin{aligned} \mathbf{Z} &= \mathbf{Z}_{\text{For}} + \mathbf{Z}_{\text{Free}} = \mathbf{AS} + \mathbf{Z}_{\text{Free}}, \\ \mathbf{S} &= \mathbf{S}_{\text{For}} + \mathbf{S}_{\text{Free}} = \mathbf{BZ} + \mathbf{S}_{\text{Free}}, \end{aligned} \quad (32)$$

resubstituting

$$\mathbf{S} = \mathbf{S}_{\text{For}} + \mathbf{S}_{\text{Free}} = \mathbf{BZ} + \mathbf{S}_{\text{Free}} \quad \text{and} \quad (33)$$

$$\mathbf{Z} = \mathbf{Z}_{\text{For}} + \mathbf{Z}_{\text{Free}} = \mathbf{AS} + \mathbf{Z}_{\text{Free}} \quad (34)$$

into the right-hand side of the two equations in (32), we obtain

$$\begin{aligned} \mathbf{Z} &= \mathbf{A}(\mathbf{BZ} + \mathbf{S}_{\text{Free}}) + \mathbf{Z}_{\text{Free}} = \mathbf{ABZ} + \mathbf{AS}_{\text{Free}} + \mathbf{Z}_{\text{Free}}, \\ \mathbf{S} &= \mathbf{B}(\mathbf{AS} + \mathbf{Z}_{\text{Free}}) + \mathbf{S}_{\text{Free}} = \mathbf{BAS} + \mathbf{BZ}_{\text{Free}} + \mathbf{S}_{\text{Free}}, \end{aligned} \quad (35)$$

if we have $\mathbf{AB} = \mathbf{I}_p$ (where \mathbf{I}_p is the identity matrix in the p -dimensional space of the \mathbf{Z}), then

$$\mathbf{0} = \mathbf{AS}_{\text{Free}} + \mathbf{Z}_{\text{Free}}, \quad (36)$$

and the forced manifold consists of the entire \mathbf{Z} dataset space

$$\mathbf{Z} = \mathbf{AS}_{\text{For}}. \quad (37)$$

Also, if $\mathbf{BA} = \mathbf{I}_q$ (where \mathbf{I}_q is the identity matrix in the q -dimensional space of the \mathbf{S}) is valid, then also the forced manifold in \mathbf{S} corresponds to the entire space. It is therefore worthwhile to discuss further the role of the product operators \mathbf{AB} and \mathbf{BA} . We can see from (35) that the \mathbf{A} and \mathbf{B} operators in generating the forced manifold gather contributions from two sectors of the respective data space. The \mathbf{A} operator generates a \mathbf{Z} forced manifold that is made up of contribution from both the \mathbf{S} forced manifold (\mathbf{AS}_{For} terms) and the $\mathbf{AS}_{\text{Free}}$ term. The latter term expresses the contribution to the \mathbf{Z} variability from \mathbf{S} variability that cannot be linked, by the inverse problem, back to the \mathbf{Z} variability itself, and it also contains the effects of nonlinearities (Fig. 6). In practice, the contribution of this term to the variability of the forced manifold is small and the EOF of the forced manifold defined as \mathbf{AS} differs very little from those of \mathbf{AS}_{For} (namely, \mathbf{ABZ}). We can think of these two operators as defining two channels, the \mathbf{S} channel and the \mathbf{Z} channel. In the \mathbf{S} channel we start from \mathbf{S} , apply \mathbf{A} to get \mathbf{Z}_{For} , then apply \mathbf{B} to go back to a subspace of \mathbf{S} that is not \mathbf{S}_{For} because of the effects of nonlinear free variability (the $\mathbf{BZ}_{\text{Free}}$ term) that we are not including. In the \mathbf{Z} channel we start from \mathbf{Z} , apply \mathbf{B} to get \mathbf{S}_{For} and then apply \mathbf{A} to get to a subspace of \mathbf{Z} .

It is instructive to investigate the detailed structure of \mathbf{AB} and \mathbf{BA} (Fig. 7). The bars indicate the value of each coefficient as before and we can see that the dominant structure is getting closer to the identity matrices; \mathbf{BA} reaches a very high value for the lowest modes, meaning that if we try to obtain the first mode from \mathbf{S} using \mathbf{A} and then use \mathbf{B} to go back to \mathbf{S} , we can do that with good reliability, but the opposite route is not so efficient. The coefficient of \mathbf{BA} for the first mode of the SST is 0.76 but is only 0.40 for the coefficient of \mathbf{AB} for the first mode of \mathbf{Z} .

It is worthwhile to note that the condition that the forced manifolds covers the entire data spaces [i.e., (36) holds and $\mathbf{AB} = \mathbf{I}_p$, $\mathbf{BA} = \mathbf{I}_q$] translates at least under CCA scaling into the relations $\mathbf{AA}' = \mathbf{I}_p$ and $\mathbf{A}'\mathbf{A} = \mathbf{I}_q$. In this case the \mathbf{A} operator would be orthogonal and the \mathbf{S} and \mathbf{Z} field could be rotated into each other. This seems to imply that the only situation in which the operator connecting the fields is orthogonal, such as those assumed by SVD and CCA, is when there is no unconnected variability in the two fields.

We can compute the values of the various terms of

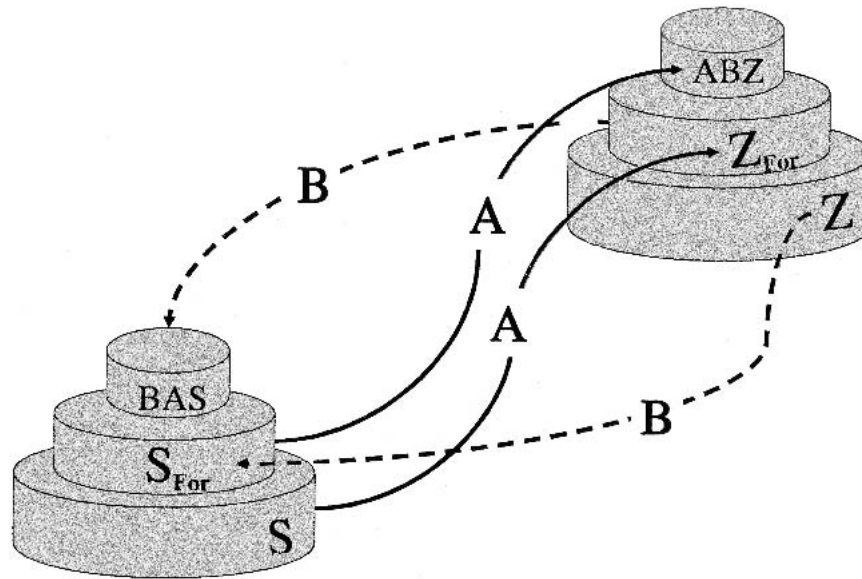


FIG. 6. A schematic of the action of the operators and of the manifolds involved in the discussion. The datasets \mathbf{S} and \mathbf{Z} are shown here to include the respective forced manifolds. The operator \mathbf{A} transforms the \mathbf{S} space into the \mathbf{Z} space, and the \mathbf{B} operators do the opposite operation. When \mathbf{A} or \mathbf{B} are applied to the entire data space (\mathbf{S} for \mathbf{A} and \mathbf{Z} for \mathbf{B}) the forced manifold is obtained. Traveling back to the original space from the forced manifolds using the appropriate operators does not result in general with the whole forced manifold. The application of the \mathbf{B} operator to the \mathbf{Z} forced manifold yields a special subset of the \mathbf{S} forced manifold, identified by \mathbf{BAS} , whereas application of the \mathbf{A} operator to the \mathbf{S} forced manifold reaches into the special subset of the \mathbf{Z} forced manifold \mathbf{ABZ} .

Eq. (35) for different regions (Table 3). The percentage of variance explained by the forced manifold gets smaller as we move to regions where the tropical Pacific SST becomes less influential. There is a small effect on the discrepancy between \mathbf{AB} and \mathbf{BA} due to the different dimension of the matrices, but if we force the matrices to have the same dimension, choosing the same number of EOFs for both fields, we get a similar result. For instance, if we elect to retain 15 EOFs each for \mathbf{S} and \mathbf{Z} , corresponding to retain 90% of the \mathbf{Z} variance and 95% of the SST variance, the values for \mathbf{ABZ} and \mathbf{BAS} for the first region (120–360) in the table become 0.20 and 0.38, respectively.

Because \mathbf{Z}_{FOR} is a time series of fields we can now apply to it also the traditional analysis tools. For instance, we can have an idea of how the forced manifold variability is composed by looking at the first three EOFs of \mathbf{Z}_{FOR} in Fig. 8. The modes illustrate the variability of the part of the field directly correlated to the SST. The modes indicate a dominant role of the SST over the Pacific–North American sector and a diminishing role of the Pacific SST over the Atlantic. The first mode (Fig. 8, top) has a distinct shape reminiscent of the Pacific–North American pattern. Center of actions are present over the Pacific, Canada, and the southeast United States. The second mode (middle panel) is also a wavelike mode, but apparently generated in the western Pacific and arching toward the

middle Atlantic. Wavelike modes can be dynamically traced to forcing from equatorial SST, but the third mode (bottom panel), a zonally elongated mode, seems to indicate variations at the entrance of the jet region. Figure 9, the first mode of the free manifold (top), shows a different picture. This mode is a almost annular mode with center of action at the exit of the jets, and the same pattern is displayed by the second mode (middle). The third mode (bottom) is instead a wavelike mode.

It is always delicate to interpret physically EOFs and it is especially so for modes higher than the first. However, it is possible to note that the modes in the free manifold, uncorrelated with the SST, have a preference for dipole modes at the exit of the jets both in the Atlantic and Pacific sector, but wavelike modes also are present, whereas the forced manifold has a preponderance of wavelike modes. This situation reflects the fact that wavelike modes can be excited both by the internal dynamics of the system and by the SST variability in tropical Pacific.

The point-by-point ratio of the variance of the forced manifold to the total variance is displayed in Fig. 10. This picture was obtained by computing the variance of forced manifold in each point dividing it by the variance of total field in that point. The top panel is for the forced manifold of the \mathbf{Z} field obtained using the \mathbf{A} operator, and the bottom panel shows the forced mani-

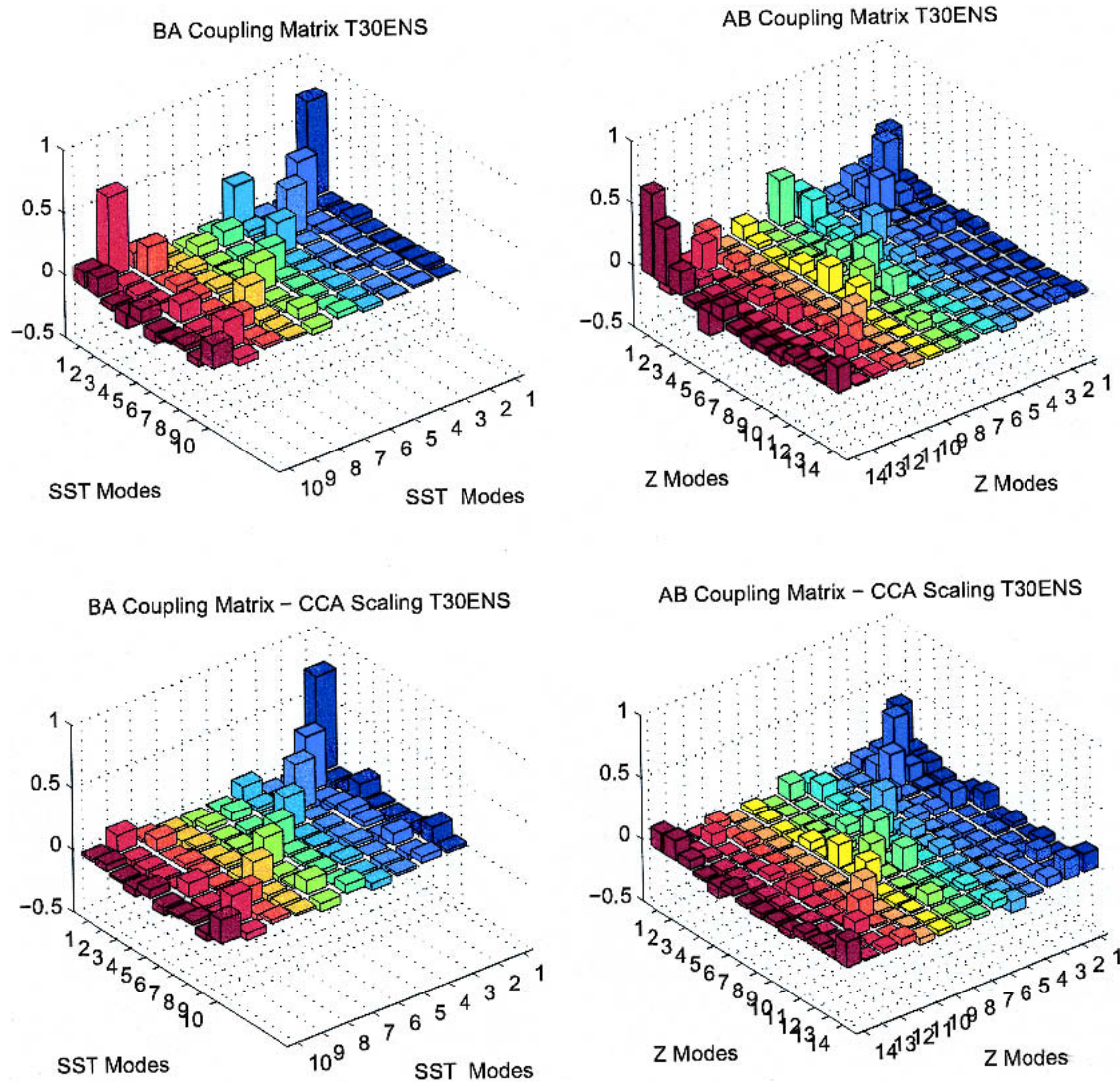


FIG. 7. The channel operators for the ensemble case. (top) For the unscaled case; (bottom) CCA-like scaling is applied. (left) The channel operators for the S channel; (right) channel operators for the Z channel. The S channel is showing that 76% of the first SST EOF mode is in the forced manifold, but the Z channel shows that only 40% of the first Z EOF mode is in the forced manifold.

fold of the **S** field computed using the **B** operator. The values indicate the fraction of the total variance that can be attributed to the forced manifold in a different spatial location. They convey some information of potential predictability maps if we assume that signals influenced by SST are predictable (Stern and Miyakoda 1995; Rowell 1998). Because of the orthogonality between the forced and free manifolds, the remaining fraction of variance must be attributed to the free manifold. In the case of the geopotential this information can also be obtained using ensemble experiments and the methods of separation of variance (Rowell 1998). This method also yields information of the amount of variance that can be ascribed to SST. A comparison between Figs. 10 and 11 indicates that the forced mani-

fold is consistent with the separation of variance method, but it obtains different patterns. In this case, the SST influence is more concentrated on North America, and weaker influence is obtained over the North Atlantic and over Eurasia.

6. The coupled manifold

The analysis of the variance induced by external fields becomes considerably more complex in the case of the analysis of a coupled model or the observations. The major complication is that we cannot use the arsenal of methods that has been extensively developed for the case of forced, mainly SST prescribed, simulations.

TABLE 3. Indices to measure the connection between the fields. The table shows the norms of the fields reconstructed using **AB** and **BA** and the other terms for Eq. (35), normalized by the norms of the total fields. A value of 1 indicates that the forced manifold includes the entire variability and that the free manifold is zero. The regions are varying only for the geopotential; the SST region (20°N–20°S, 120°–290°E) is being kept fixed in all cases. The first two columns in each case indicate the forced manifold.

Regions	Geopotential Z			SST		
	Forced manifold		Free manifold	Forced manifold		Free manifold
Longitudes	ABZ	AS_{Free}	Z_{Free}	BAS	BZ_{Free}	S_{Free}
120°–360°	0.17	0.13	0.70	0.38	0.16	0.46
0°–120°	0.08	0.11	0.80	0.17	0.14	0.69
300°–360°	0.07	0.15	0.78	0.11	0.13	0.76
60°–120°	0.08	0.13	0.78	0.13	0.14	0.73

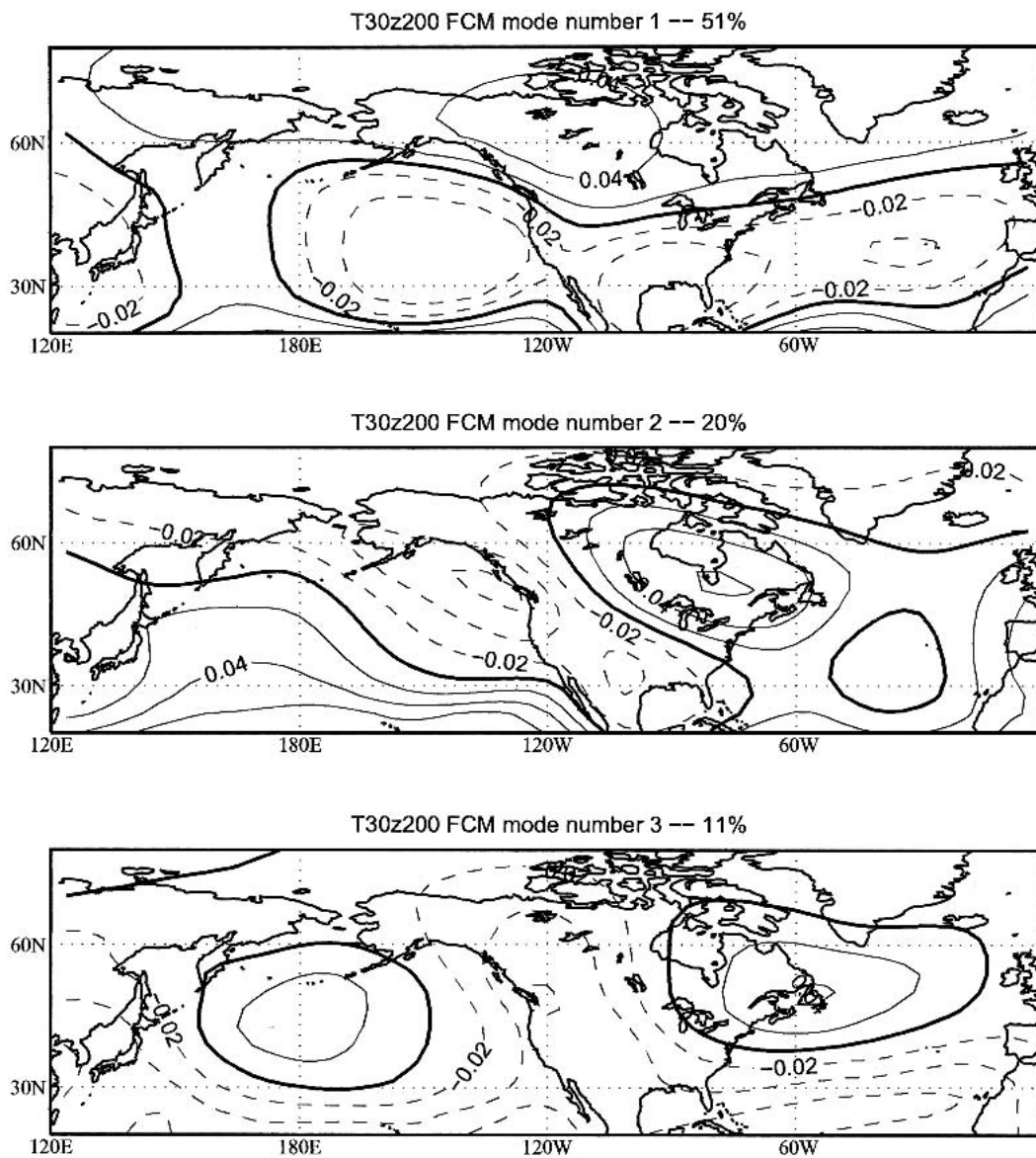


FIG. 8. First three EOFs of the forced manifold of the geopotential for the ensemble case. Negative contours are dashed, and the contour interval is arbitrary.

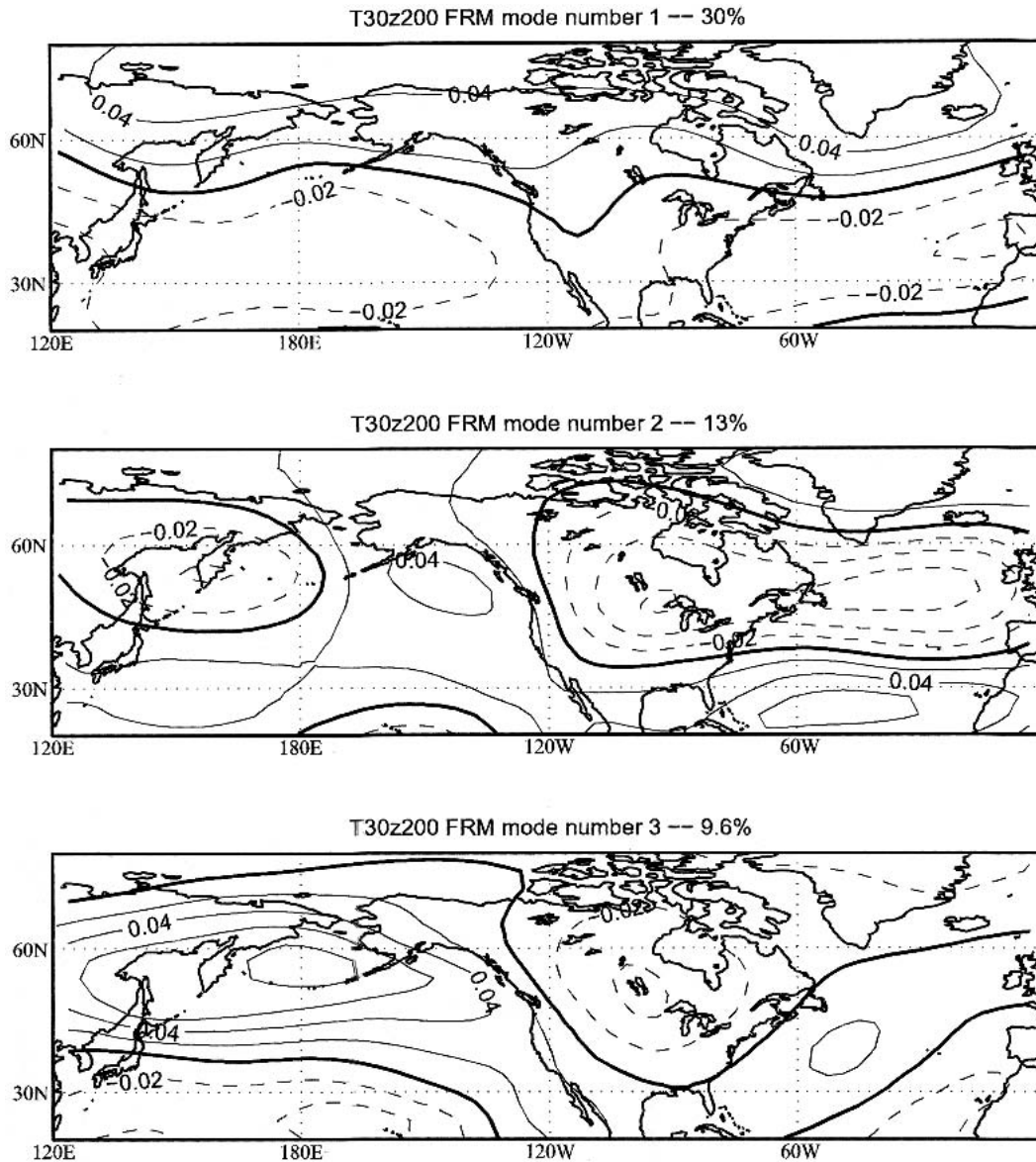


FIG. 9. As in Fig. 8, but for the free manifold of the geopotential.

The definition of ensemble itself becomes troublesome, maybe impossible. It is particularly difficult in the case of the analysis of coupled atmosphere–ocean dynamics in the context of coupled model experiments. In this case the ensemble approach fails because we do not have the repetition of different atmospheric responses to the same SST that is at the core of the separation between forced and free variance. The PRO method, however, is sufficiently general that we can use it as the core of a method to separate forced and free variability also in the coupled case.

The PRO method can overcome this difficulty because we can set the same minimization problem as in the prescribed SST case. We can apply either Eq. (3) or Eq. (9) to the SST from the coupled model and to the

selected atmospheric field and also the practical, faster method [Eq. (12)] can be applied easily.

The data fields in this case consist of single realizations from a coupled numerical experiment or the observations. The main problem in this case is the possibility of overfitting because of the incorrect estimation of the linear relations among the data fields. In practice, the rank of the data matrix will be numerically different from zero, but from the physical point of view many modes will be redundant and they will not contribute to the physical variance of the field. The problem would not reveal itself in the previous case because the **S** data matrix in an ensemble of experiments with prescribed forcing like SST is rank deficient by construction not only physically but also mathematically, because of the

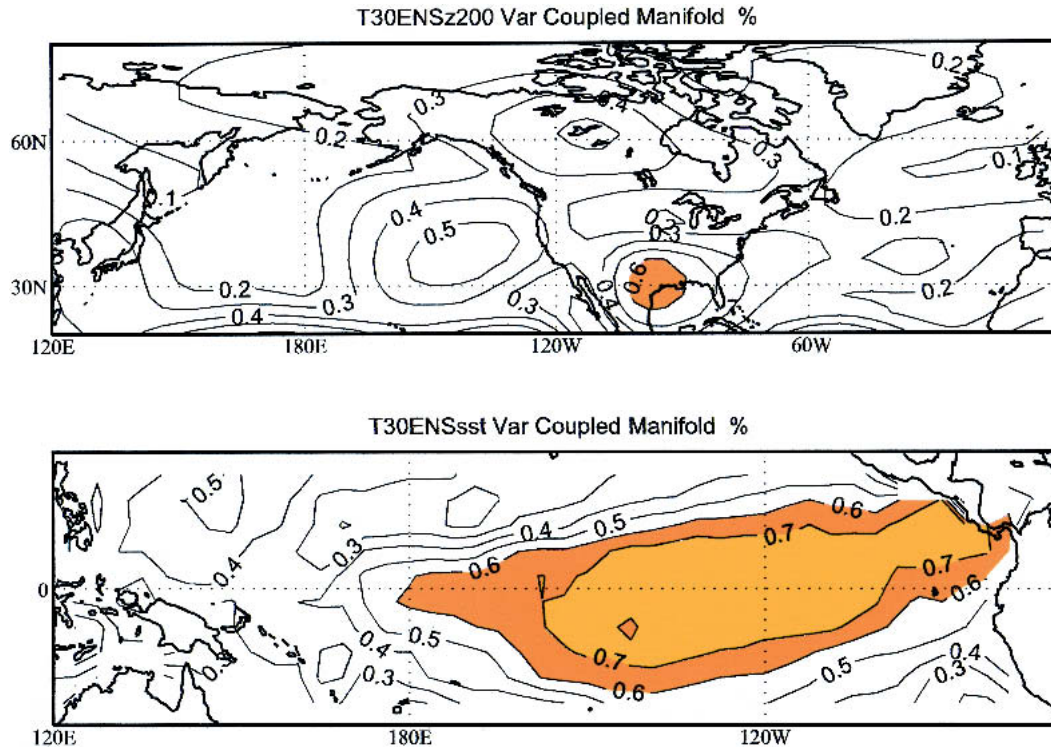


FIG. 10. Ratio of the forced manifold variance to the total variance for (top) the SST and (bottom) the geopotential. The contour interval is 0.1.

repeated instances of the same SST for different members of the ensemble.

With the single realization of the coupled or observed case, the EOF analysis can easily identify these modes by ranking them in terms of explained variance, so we can use the fast practical method to prefilter the data-eliminating modes that explain very little of the variance. This procedure is similar to the one that has been used in the Barnett–Preisendorfer CCA (Barnett and Preisendorfer 1978), and the criteria used for selecting the EOF can also be used in this case. In the following, we demonstrate this effect using the observed surface zonal stresses from the National Centers for Environmental Prediction (NCEP) reanalysis for

the period 1951–2000 and the SST from the Hadley Centre Sea Ice and SST (HadISST) dataset for the same period.

The application of this method to the observed Z200 and SST fields is shown in Fig. 12. We have here retained EOFs that represent 90% of the variance in both cases. The Z200 pattern shows strong similarities to the model case, but there are also some interesting differences, such as the secondary maximum over northern Japan. The SST, on the other hand, is very similar to the model case, except for an area in the western Pacific. This seems to indicate that the areas that are forcing the atmosphere are roughly the same, but the response of the model is simpler than the atmosphere. However, a

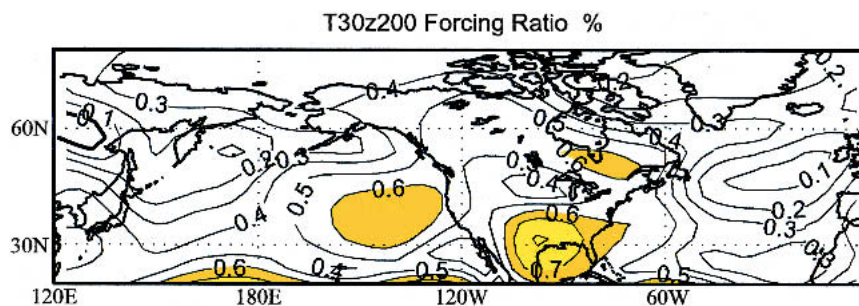


FIG. 11. Ratio of the forced variance to the total variance according to the separation of variance method. The contour is 0.1.

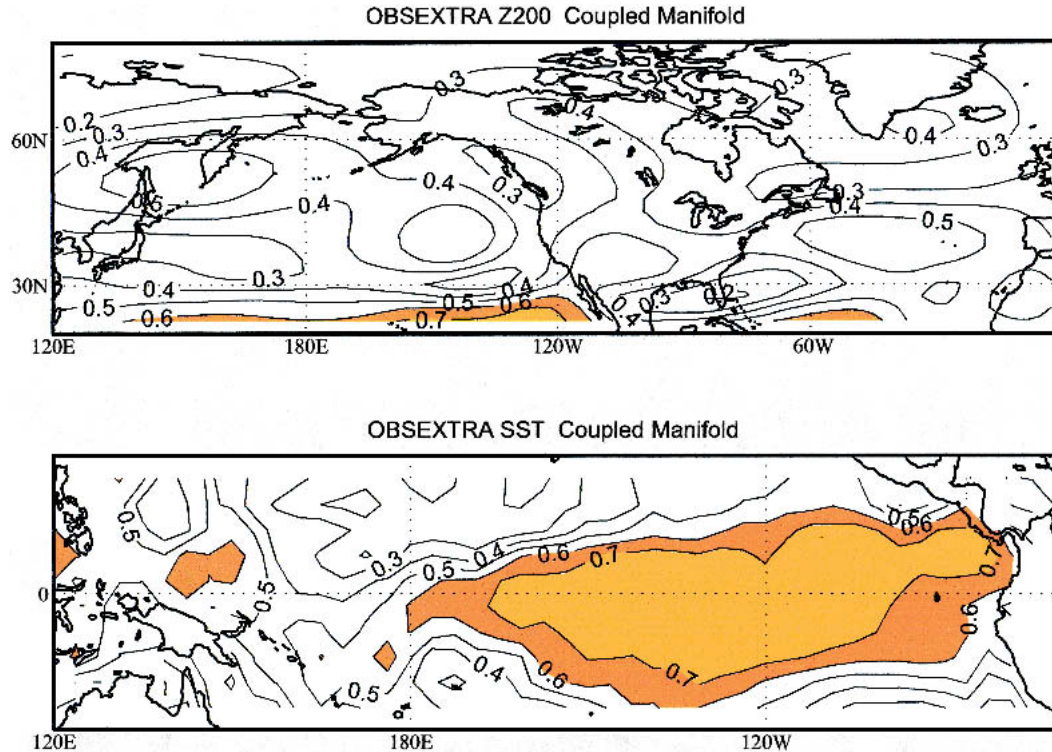


FIG. 12. Ratio of the forced manifold variance to the total variance for the observations case for (top) the SST and (bottom) the geopotential. The observations used here are the NCEP reanalysis data 1950–2000 for the geopotential at 200 mb and the HadISST for the same periods. The contour interval is 0.2.

definitive interpretation of this pattern will require more extended investigation. It is sufficient here to show that the method can be applied to observations, that is, a single realization.

It is interesting to test the PRO method in a case in which we have to consider more tightly coupled physical variables than Z200 and SST. A good example is applying the method to tropical surface zonal stress from the NCEP reanalysis as the **Z** field and the HadISST as the **S** field. Some years ago during the development of hybrid models for ENSO forecasting and/or simulations multiple regression between stresses and SST had been considered (see, e.g., Eckert and Latif 1997), in some cases also using SVD between EOF coefficients of the stresses and SST (Syu et al. 1995). However, the general context and the potential of this formulation has been overlooked.

Using the methods developed in the preceding section we obtain the results shown in Table 4, which shows the dependence of the forced manifold on the amount of variance retained in the preanalysis of the fields on their own EOFs. The forced manifolds explain 50%–60% of the variance. We can see the effect of working with a single realization. As the variance retained increases, the indices become closer to unity, indicating that the manifold obtained via the **A** or **B** operator from the **S** or **Z** field tend to coincide with the

totality of the data. This manifold is the analog of the forced manifold of the previous section, but in this case it is more symmetric: both indices are giving closer values, indicating that the fields can be reconstructed one from the other. In this sense this is not a forced manifold, but we might call it a *coupled manifold*. If we choose to keep fixed the number of EOFs retained for each field, rather than the overall variance, we get similar results (Table 5).

The elimination of the noise by the Barnett–Preisendorfer procedure is very beneficial; as we can see from the inspection of the **A** and **B** influence ma-

TABLE 4. Indices for the extent to which the fields are connected to each other for the observations. The table shows the norms of the fields reconstructed using **AB** and **BA** and the other terms for Eq. (35), normalized by the norms of the total fields, for different amounts of retained variance. A value of 1 indicates that the forced manifold includes the entire variability and that the free manifold is zero. The variance retained (Var Ret) is the same for both fields.

Var Ret	U stress			SST		
	ABZ	AS _{Free}	Z _{Free}	BAS	BZ _{Free}	S _{Free}
60%	0.30	0.12	0.57	0.50	0.16	0.34
70%	0.33	0.12	0.54	0.55	0.16	0.28
80%	0.37	0.12	0.50	0.56	0.15	0.29
90%	0.49	0.09	0.42	0.65	0.12	0.23

TABLE 5. As in Table 4, but for the case in which the number of EOFs retained in each field is the same. The behavior is more symmetric.

EOF retained (%)	Indices	
	ABZ	BAS
4: Z 49%, S 64%	0.31	0.42
5: Z 55%, S 70%	0.37	0.47
8: Z 66%, S 81%	0.41	0.48
14: Z 80%, S 91%	0.48	0.55

trices, the higher modes tend to dominate if we include all of them, especially in the S channel (the **A** matrix). The CCA scaling will remove the effect of variance and results in more balanced distribution, with a clustering toward the lower modes.

The sensitivity to various regions is analyzed in Table 6, where we have calculated the coupled manifold for several regions outside the Tropics. The SST reference region in the tropical Pacific has been similarly main-

TABLE 6. Indices for the sensitivity to the region. The regions have been modified for the **U** stress only, whereas the SSTs are always for the region (20°N–20°S, 120°–290°E); the A region is (70°–40°S, 300°–360°E); the B region is (40°–70°N, 300°–360°E); the C region is (70°–40°S, 140°–290°E); the D region is (30°–70°N, 140°–230°E).

Region	U stress			SST		
	ABZ	AS _{Free}	Z _{Free}	BAS	BZ _{Free}	S _{Free}
A: South Atlantic	0.26	0.15	0.60	0.22	0.13	0.65
B: North Atlantic	0.20	0.20	0.60	0.08	0.10	0.83
C: South Pacific	0.30	0.16	0.55	0.28	0.15	0.57
D: North Pacific	0.38	0.15	0.47	0.30	0.12	0.57

tained, but various areas for the zonal stresses have been considered in the North and South Atlantic and Pacific Oceans. The coupling manifolds are getting smaller as we depart for the tropical Pacific as more of the variability of the zonal stresses tends to be poorly connected to the SST tropical variability. It is interesting that the nonlinear influences (the **AS_{Free}** term) have

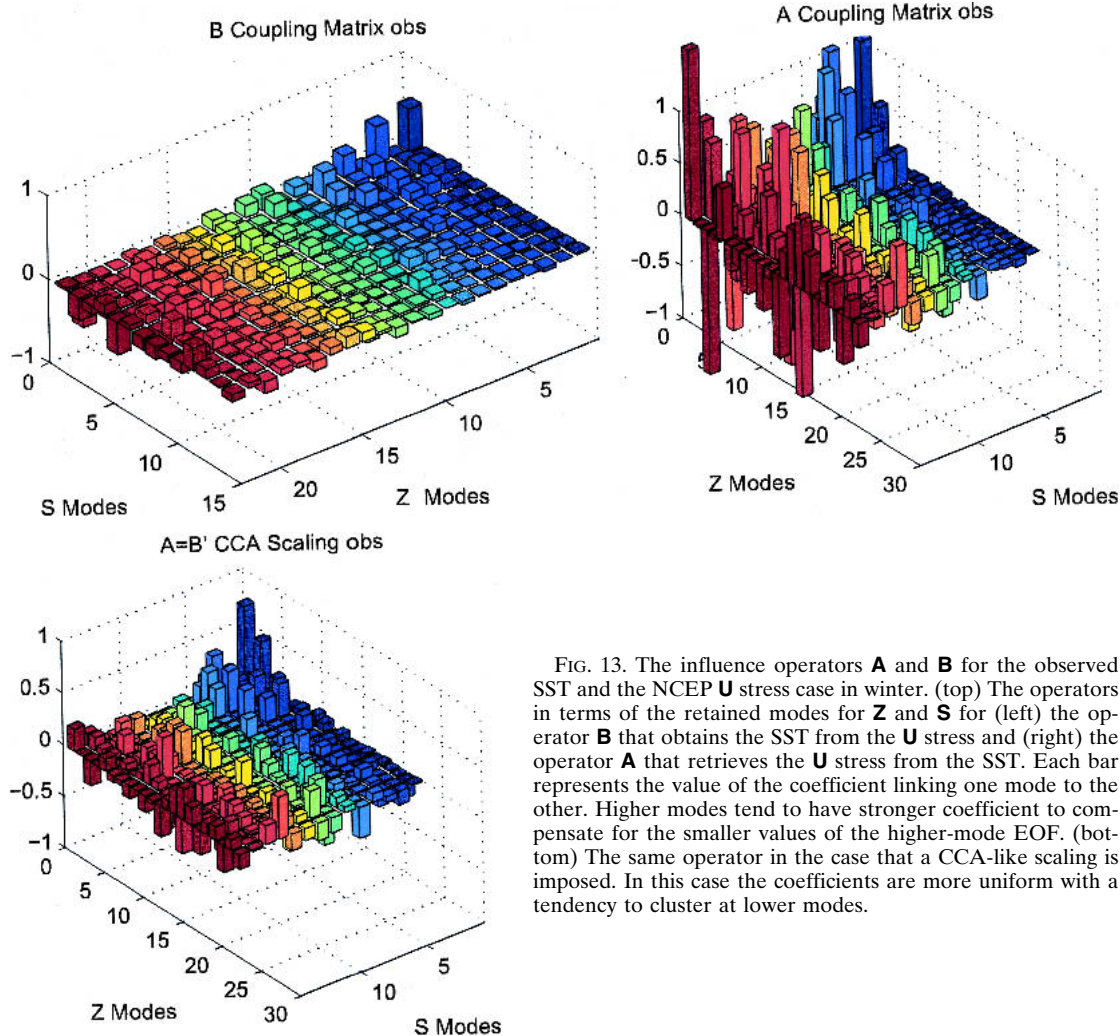


FIG. 13. The influence operators **A** and **B** for the observed SST and the NCEP **U** stress case in winter. (top) The operators in terms of the retained modes for **Z** and **S** for (left) the operator **B** that obtains the SST from the **U** stress and (right) the operator **A** that retrieves the **U** stress from the SST. Each bar represents the value of the coefficient linking one mode to the other. Higher modes tend to have stronger coefficient to compensate for the smaller values of the higher-mode EOF. (bottom) The same operator in the case that a CCA-like scaling is imposed. In this case the coefficients are more uniform with a tendency to cluster at lower modes.

a peak in the North Atlantic, presumably via an influence on the storm-track activity over the North American sector. Figure 13 shows the influence operators for the observations of zonal stresses and SST. Also in this case the effect of different weights of the EOF with respect to the variability can be removed via a CCA-like scaling. The result is a more balanced distribution with a clustering of large coefficients toward the lower modes. The channel operators **AB** and **BA** (Fig. 14) show that the S channel and the Z channels are more symmetric and the recovery of the coupled manifold is quite feasible. The first mode of the stresses in the Z channel can be recovered with a coefficient of 0.83, and the corresponding coefficient for the first mode of the SST in the S channel has a comparative value of 0.90. The fields can be recovered from one another easily.

The first EOF of the coupled manifold (Fig. 15) of the zonal stresses shows a mode with an equatorial concentration, but the other modes display off-equatorial centers of action. The modes of the coupled manifold for the SST (Fig. 16) display a wide tropical mode and a tight equatorial mode. The modes of the coupled manifold are different from those identified via an EOF analysis of the total field, being separated into a large tropical mode and a dipolar mode along the Pacific. The difference is particularly noticeable in the zonal stresses, whereas in the SST, it is less dramatic.

The fraction of variance of the zonal stresses that can be explained in terms of SST and vice versa is shown in Fig. 17. The picture reveals clearly the areas where the zonal stresses are closely coupled to the SST, and some interesting details emerge, such as the identification of

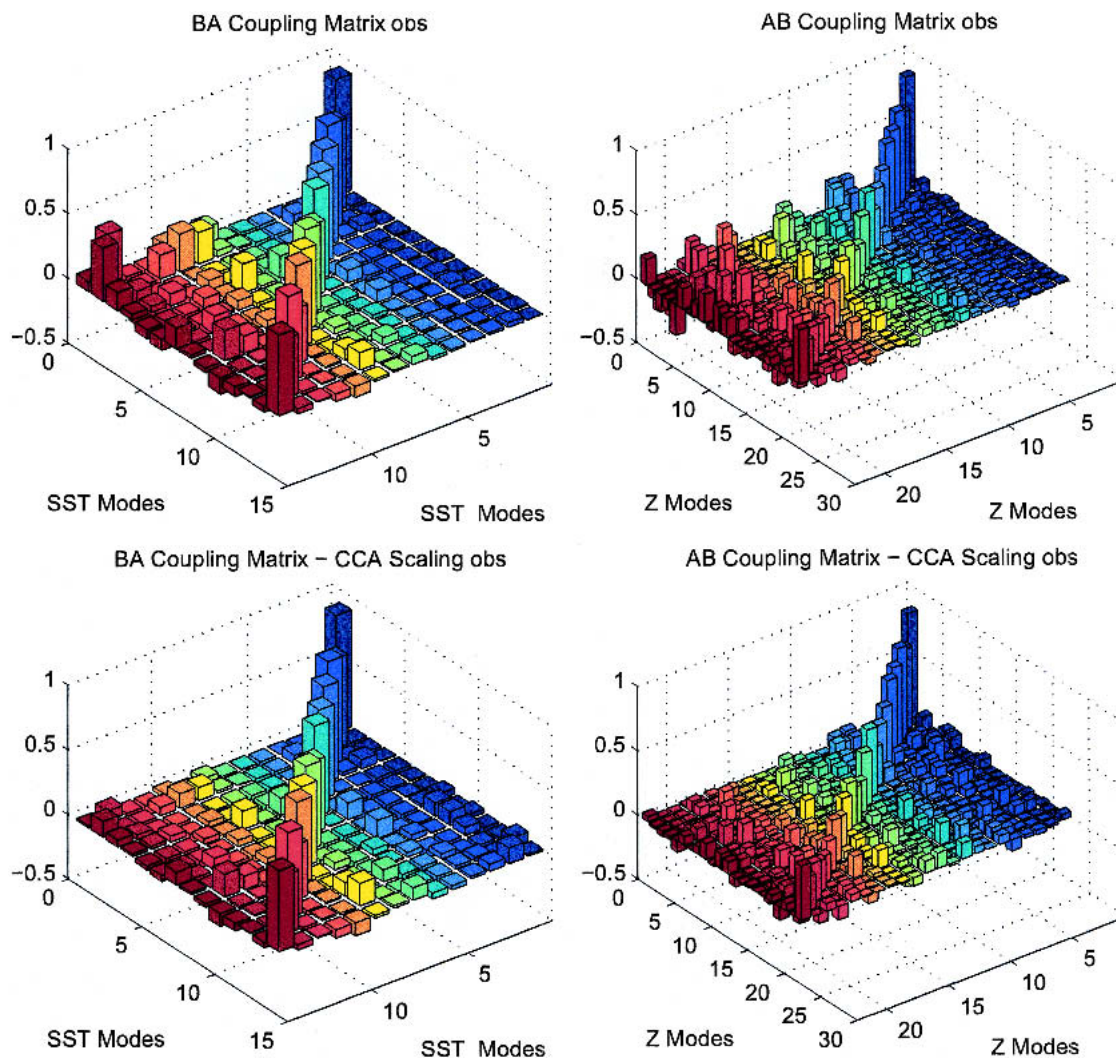


FIG. 14. The channel operators for the coupled case: (top) for the unscaled case and (bottom) CCA-like scaling is applied. The channel operators for (left) the S channel, and (right) the Z channel. The S channel is showing that 83% of the first SST EOF mode is in the forced manifold, but the Z channel shows that only 90% of the first stress EOF mode is in the forced manifold.

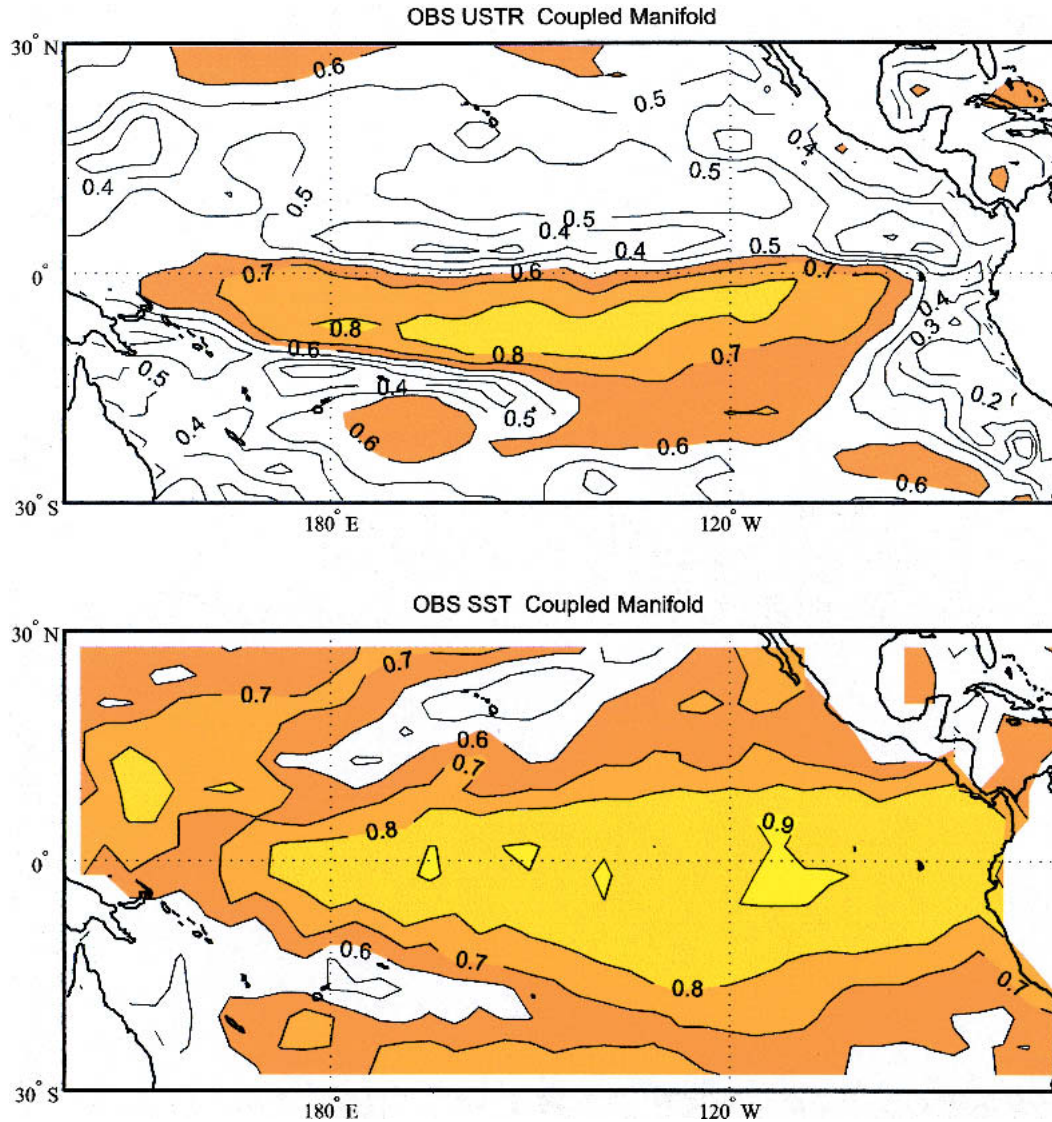


FIG. 15. EOF of the coupled manifold of the \mathbf{U} component of the surface stress for the observations. Negative contours are dashed, and the contour interval is arbitrary.

the strongly coupled areas in the central Pacific just south of the equator. This field can be considered as the generalization to the coupled or observation case of the potential predictability estimation that can be done using ensembles.

7. Discussion and conclusions

The manifolds that can be identified by the usage of the PRO method offer the possibility to detect the existence of coupled variability in a more general context and with a more natural set of hypotheses, overcoming some of the limitations of the SVD and CCA methods. The forced manifold in the case of prescribed boundary forcing experiments is consistent with other methods of

estimating the SST-related variance, but it can yield the time series of the various data fields that are related to each other. Furthermore, the splitting of the field in forced and free manifolds is orthogonal, and the free manifold is by construction independent of the other field. The removal of the impact of the \mathbf{S} field is therefore more complete than with the other methods, such as using an ensemble mean to estimate the forced manifold. We have also shown that the manifolds are distinct sectors of the variance of the fields, since their EOF are distinct from those of the entire field. The modes bring of course the signature of the main mode of variations, but they are distinct.

The method and the concepts can be generalized to the observations or to coupled simulations, yielding the

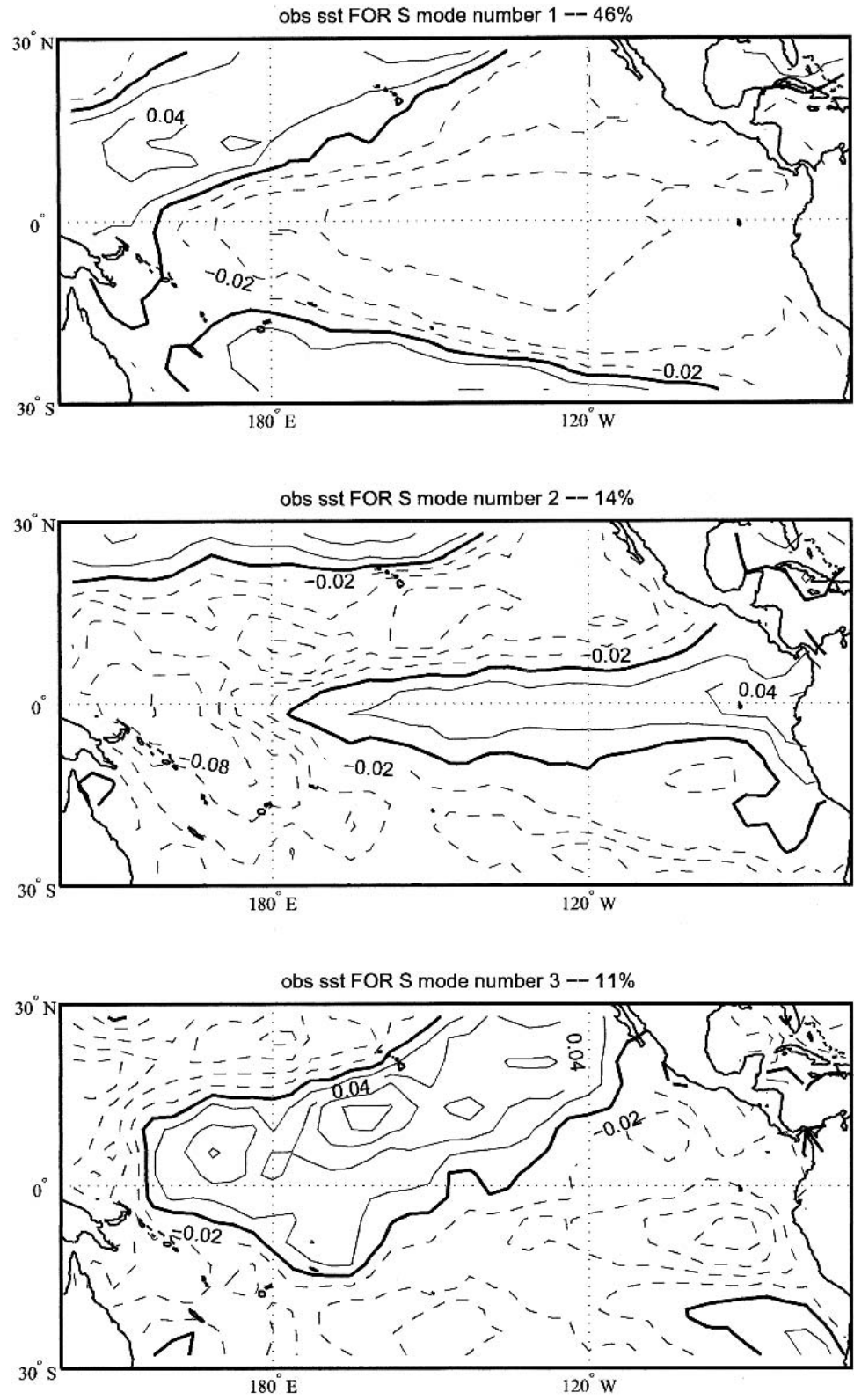


FIG. 16. As in Fig. 15, but for the coupled manifold of the SST.

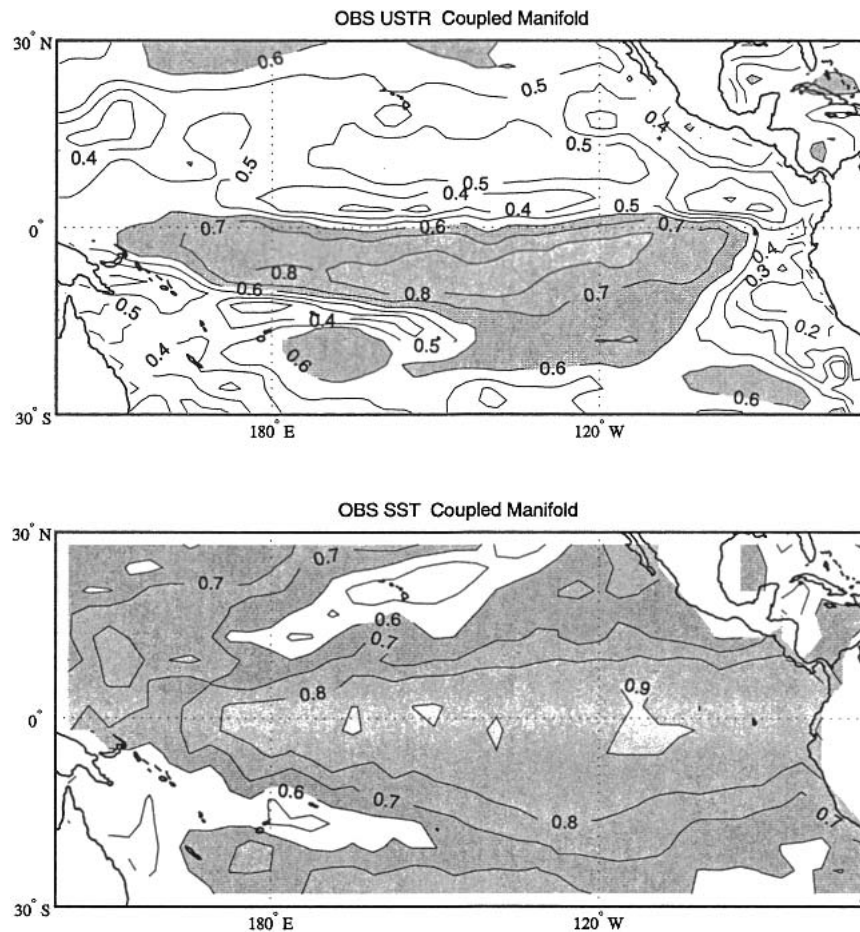


FIG. 17. Ratio of the coupled manifold variance to the total variance for (top) the zonal \mathbf{U} stress and (bottom) the SST. The contour interval is 0.2.

possibility of estimating the forced variance, in this case the coupled variance, linking two fields and the nature of their reciprocal relationship. The possibility of estimating the coupled variance will allow the extension of the potential predictability to the coupled model context. The concept of potential predictability in the context of long coupled simulations needs discussion since it must be considered as essentially the ratio of the coupled variance to the total variance. It is in fact the coupled portion of the variance that can give rise to the estimation of potential predictability in the coupled context. The method described in this paper can also be useful in the case of analysis of traditional ensembles with coupled models, such as for instance the case of coupled simulations forced by the same time and space distribution of greenhouse forcing gases, but with different initial conditions.

Acknowledgments. This work was completed with the support of the Italy–U.S. Cooperation Program in Climate Science and Technology funded by the Italian Ministry of Environment and Territory.

REFERENCES

- Barnett, T. P., 1995: Monte Carlo climate forecasting. *J. Climate*, **8**, 1005–1022.
- , and R. W. Preisendorfer, 1978: Multifield analog prediction of short-term climate fluctuations using a climate state vector. *J. Atmos. Sci.*, **35**, 1771–1787.
- Bretherton, C. S., C. Smith, and J. M. Wallace, 1992: An intercomparison of methods for finding coupled patterns in climate data. *J. Climate*, **5**, 371–389.
- Brier, G. W., and G. T. Meltesen, 1976: Eigenvector analysis for prediction of time series. *J. Appl. Meteor.*, **15**, 1307–1312.
- Cheng, X., and T. J. Dunkerton, 1995: Orthogonal rotation of spatial patterns derived from singular value decomposition analysis. *J. Climate*, **8**, 2631–2643.
- Cherchi, A., and A. Navarra, 2003: Reproducibility and predictability of the Asian summer monsoon in the ECHAM4-GCM. *Climate Dyn.*, **20**, 365–379.
- Cherry, S., 1996: Singular value decomposition and canonical correlation analysis. *J. Climate*, **9**, 2003–2009.
- , 1997: Some comments on the singular value decomposition analysis. *J. Climate*, **10**, 1759–1761.
- Eckert, C., and M. Latif, 1997: Predictability of a stochastically forced hybrid coupled model of El Niño. *J. Climate*, **10**, 1488–1504.
- Gates, W. L., 1992: AMIP: The atmospheric model intercomparison project. *Bull. Amer. Meteor. Soc.*, **73**, 1962–1970.

- Golub, G. H., and C. F. van Loan, 1989: *Matrix Computations*. 2d ed. Johns Hopkins University Press, 642 pp.
- Graham, N. E., T. P. Barnett, R. Wilde, M. Ponater, and S. Schubert, 1994: On the roles of tropical and midlatitudes SSTs in forcing interannual to interdecadal variability in the winter Northern Hemisphere circulation. *J. Climate*, **7**, 1416–1440.
- Harzallah, A., and R. Sadourny, 1995: Internal versus SST-forced atmospheric variability as simulated by an atmospheric general circulation model. *J. Climate*, **8**, 474–495.
- Horn, R., and C. R. Johnson, 1991: *Topics in Matrix Analysis*. Cambridge University Press, 608 pp.
- Hu, Q., 1997: On the uniqueness of the singular value decomposition in meteorological applications. *J. Climate*, **10**, 1762–1766.
- Kiladis, G. N., and H. F. Diaz, 1989: Global climate anomalies associated with extremes of the Southern Oscillation. *J. Climate*, **2**, 1069–1090.
- Kumar, A., M. Hoerling, A. Ji, A. Leetma, and P. Sardeshmukh, 1996: Assessing a GCM's suitability for making seasonal predictions. *J. Climate*, **9**, 115–129.
- Lau, N.-C., 1985: Modeling the seasonal dependence of the atmospheric response to observed El Niños in 1962–76. *Mon. Wea. Rev.*, **113**, 1970–1996.
- , and M. J. Nath, 1990: A general circulation model study of the atmospheric response to extratropical SST anomalies observed during 1950–79. *J. Climate*, **3**, 965–989.
- , and —, 1994: A modeling study of the relative roles of tropical and extratropical SST anomalies in the variability of the global atmosphere–ocean system. *J. Climate*, **7**, 1184–1207.
- Moron, V., A. Navarra, M. N. Ward, and E. Roeckner, 1998: Skill and reproducibility of seasonal rainfall patterns in the Tropics in ECHAM4 simulations with prescribed SST. *Climate Dyn.*, **14**, 83–100.
- Newman, M., and P. D. Sardeshmukh, 1995: A caveat concerning singular value decomposition. *J. Climate*, **8**, 352–360.
- North, G. R., T. L. Bell, and R. F. Cahalan, 1982: Sampling errors in the estimation of empirical orthogonal functions. *Mon. Wea. Rev.*, **110**, 699–706.
- Rayner, N. A., E. B. Horton, D. E. Parker, C. K. Folland, and R. B. Hackett, 1996: Version 2.2 of the global sea-ice and sea surface temperature data set, 1903–1994. Climate Research Tech. Note 74, Hadley Centre for Climate Prediction and Research, United Kingdom, 21 pp.
- Richman, M. B., and S. J. Vermette, 1993: The use of Procrustes target analysis to discriminate dominant source regions of fine sulfur in the western USA. *Atmos. Environ.*, **27A**, 475–481.
- Roeckner, E., and K. Arpe, 1995: AMIP experiments with the new Max Planck Institute Model ECHAM4. *Proc. First Int. AMIP Scientific Conf.*, Monterey, CA, WRCP-92, WMO Tech. Doc. 732, 307–312.
- , and Coauthors, 1996: The atmospheric general circulation model ECHAM-4: Model description and simulation of present-day climate. Rep. 218, MPI, Hamburg, Germany, 90 pp.
- Ropelewski, C. F., and M. S. Halpert, 1987: Global and regional scale precipitation patterns associated with the El Niño/Southern Oscillation. *Mon. Wea. Rev.*, **115**, 1606–1623.
- , and —, 1989: Precipitation patterns associated with the high index phase of the Southern Oscillation. *J. Climate*, **2**, 268–284.
- Rowell, D. P., 1998: Assessing potential seasonal predictability with an ensemble of multidecadal GCM simulations. *J. Climate*, **11**, 109–120.
- Rowntree, P. R., 1972: The influence of tropical east Pacific Ocean temperatures on the atmosphere. *Quart. J. Roy. Meteor. Soc.*, **98**, 290–291.
- Shukla, J., and Coauthors, 2000: Dynamical seasonal prediction. *Bull. Amer. Meteor. Soc.*, **81**, 2593–2606.
- Sperber, K. R., and T. N. Palmer, 1996: Interannual tropical rainfall variability in general circulation model simulations associated with the Atmospheric Model Intercomparison Project. *J. Climate*, **9**, 2727–2750.
- Stern, W., and K. Miyakoda, 1995: Feasibility of seasonal forecasts inferred from multiple GCM simulations. *J. Climate*, **8**, 1071–1085.
- Syu, H.-H., J. D. Neelin, and D. Gutzler, 1995: Seasonal and interannual variability in a hybrid coupled GCM. *J. Climate*, **8**, 2121–2143.
- Venzke, S., M. R. Allan, R. T. Sutton, and D. P. Rowell, 1999: The atmospheric response over the North Atlantic to decadal changes in sea surface temperature. *J. Climate*, **12**, 2562–2584.

CORRIGENDUM NOTE

Figures 15 and 17 are not correct as shown above. A corrigendum with the correct figures will be published in the May 2005 issue.